INFRARED STUDY OF GROUP V HEXAFLUORIDE FULLERIDES

INFRARED STUDY OF GROUP V HEXAFLUORIDE FULLERIDES

By

RONALD L. FRANCIS, B.Sc.

A Thesis

Submitted to the School of Graduate Studies

in Partial Fulfilment of the Requirements

for the Degree

Master of Science

McMaster University

MASTER OF SCIENCE (1996) McMaster University
(Physics) Hamilton, Ontario

TITLE: Infrared Study of Group V Hexafluoride Fullerides

AUTHOR: Ronald L. Francis, B.Sc. (York University)

SUPERVISOR: Professor W. R. Datars

PAGES: *x*, 76

ABSTRACT

Acceptor compounds of C_{60} and hexafluoride ions of group V elements (P, As, Sb) were studied by infrared spectroscopy, x-ray diffraction and resistivity measurements. $C_{60}(AsF_6)_{1.9}$ was formed by reacting C_{60} powder with AsF_5 gas dissolved in liquid SO_2. The AsF_6^- ion was identified by a broad ν_3 absorption at 703 cm^{-1}, a shoulder at 681 cm^{-1} and evidence of the sharp ν_4 absorption just below 400 cm^{-1} in the infrared spectrum. The low frequency modes of C_{60} at 527 and 576 cm^{-1} were unshifted in the reacted powder. The $T_{1u}(3)$ mode of C_{60}, at 1183 cm^{-1}, was accompanied by neighbouring absorptions at 1194 and 1206 cm^{-1}, which were assigned tentatively to splitting of the triply degenerate mode. Three strong broad peaks at 1549, 1406 and 1322 cm^{-1} observed in the spectra were assigned to splitting of the threefold degenerate $T_{1u}(4)$ mode of pristine C_{60} at 1428 cm^{-1}. Heat treatments of the sample, with temperatures ranging up to 350°C, were performed to thermally deintercalate the sample and to aid in identifying the infrared modes. The decrease in intensity of the AsF_6^- absorptions and the return of the four strong absorption lines of undoped C_{60} indicated the successful deintercalation of the sample. X-ray diffraction indicated that the C_{60} lattice, which had expanded to body centered tetragonal to accommodate the AsF_6^- ion, returned to the face centered cubic arrangement of pristine C_{60} following heat treatments at 350°C. The $C_{60}(AsF_6)_{1.9}$ compound exhibited semiconductor characteristics with an activation energy of 0.12 ± 0.05 eV. Possible

interstitial sites for the AsF_6^- ion in the body-centered-tetragonal lattice of $C_{60}(AsF_6)_{1.9}$ have also been calculated.

The PF_6^- ion, in the sample of C_{60} reacted with NO_2PF_6 in SO_2, was observed in the IR spectra by the broad ν_3 absorption at 830 cm^{-1} and the sharp ν_4 absorption at 558 cm^{-1}. No strong absorption of NO_2^+ at 2360 cm^{-1} was observed indicating that the sample was not a simple mixture of the two powders. The C_{60} absorption lines, at 527, 576, 1183 and 1428 cm^{-1} were unshifted. However, the $T_{1u}(4)$ mode at 1428 cm^{-1} showed asymmetric broadening on the low frequency side and small absorptions flanking the $T_{1u}(4)$ mode. These features, although much less pronounced, may correspond to the shifting and splitting observed in the $T_{1u}(4)$ mode of the $C_{60}(AsF_6)_{1.9}$ compound. The octahedral SbF_6^- ion was identified in the sample of C_{60} powder reacted with NO_2SbF_6 by the strong ν_3 absorption at 660 cm^{-1}. The C_{60} lines were unshifted, but small absorptions flanking the $T_{1u}(4)$ mode, are again similar to the absorptions assigned to splitting in the $C_{60}(AsF_6)_{1.9}$ compound.

ACKNOWLEDGEMENTS

Although writing a thesis is by nature an individual activity, it is not a solitary one, for I could not have completed this thesis alone. I wish to express my sincere gratitude to my supervisor, Dr. W. Ross Datars, for his guidance throughout the course of this research. A special thanks goes to Dr. Pash Ummat, not only for sharing his meticulous sample preparation techniques but also for his enthusiasm and encouragement. A sincere "thank you" to Tadek Olech, and Jason Palidwar for superb technical assistance, and intriguing discussions.

It is a pleasure to have the opportunity to thank the Department of Physics, and all those within it, for offering such a stimulating environment both academically and socially. I greatly appreciate the friendship of all those who have made my stay interesting and enjoyable. I express my love and deepest gratitude to Mom and Dad for their support and encouragement. Loving thanks also to Sonia. Her encouragement and patience have been generous and indispensable.

TABLE OF CONTENTS

LIST OF TABLES

LIST OF FIGURES

We have a habit in writing articles published in scientific journals to make the work as finished as possible, to cover up all the tracks, to not worry about the blind alleys or describe how you had the wrong idea first, and so on. So there isn't any place to publish, in a dignified manner, what you actually did in order to get to do the work.

Richard P. Feynman, Nobel Lecture 1966

Chapter 1

INTRODUCTION

Research on the properties of the molecule *buckminsterfullerene*, C_{60} ,and its compounds has been increasing rapidly. Among the many synthesized materials, however, intercalated compounds of C_{60} reacted with acceptor molecules have received little attention.

The intercalation of alkali metal donors in C_{60} solid has been well established. In these materials, the alkali metal ions fit into the large octahedral and tetrahedral sites of the fcc lattice. These compounds exhibit almost complete charge transfer, leaving the C_{60} molecule in a negatively charged state. The discovery of superconductivity in potassium doped C_{60} at 18 K [Hebard, 1991] was an unexpected observation that caused an explosion in condensed matter research. With critical transition temperatures (T_c) now exceeding 30 K, the alkali metal doped fullerene superconductors are surpassed only by the copper oxide materials. All the known alkali metal doped C_{60} superconductors have the same stoichiometry, A_3C_{60}. Although there are other structurally known alkali metal doped fullerene materials, such as the body centered tettragonal (bct) phases of A_4C_{60} and the body centered cubic (bcc) phase of A_6C_{60}, these phases are insulating.

The low ionization potential of the C_{60} molecule also suggests intercalation of the solid with acceptor molecules, however few of these materials have been reported. A good candidate for an electron acceptor in C_{60}, arsenic pentafluoride, has been found to

react with graphite to form graphite intercalation compounds having electrical conductivity as high as that of silver. A reaction between C_{60} and AsF_5 was first reported in 1994 [Datars, 1994]. The material was characterized by X-ray diffraction, mass spectra analysis and nuclear magnetic resonance. The new compound, like the alkali metal fullerides, was observed to be air sensitive making study of the material somewhat difficult. The study of the infrared spectra of the material, using a sealed cell with KBr windows to contain the air sensitive sample, revealed a large absorption at 702 cm^{-1}, characteristic of the AsF_6^- ion. This lead to a proposed composition of $C_{60}(AsF_6)_{1.9}$ [Datars, 1995]. However, the sealed cell was hindered by low transmission and only two (of the four) absorption lines from C_{60} were resolved clear enough to report. Even with evidence from the other techniques, the existence of the compound was called into question due to the poorly resolved C_{60} lines in the IR specta.

Infrared spectroscopy is a powerful means of analysing the composition of new materials and has been used to study the intercalation process and the doped state of the fullerene salts. But, so far, infrared studies have concentrated almost exclusively on the alkali metal fullerides. The four infrared active T_{1u} modes are significant features in the undoped material and their response to intercalation has been important in the characterization process.

The main objective of this research project was to acquire further evidence supporting the existence of this C_{60} acceptor material. This consisted of acquiring infrared transmission spectra of the $C_{60}(AsF_6)_{1.9}$ compound using a specially constructed apparatus

to contain the air sensitive samples. Also, in an attempt to drive off the intercalant, heat treatments of the sample were performed in vacuum. Temperatures ranged up to 350°C, with infrared spectra of the powder being taken at certain intervals (after cooling again to room temperature). Sealed cells were also used to conduct resistivity measurements and to obtain further X-ray diffraction data.

As well, reactions were carried out in an attempt to intercalate solid C_{60} with other group V hexafluoride ions . It was realized that both the ν_3 and ν_4 modes of the octahedral PF_6^- ion could be observed within the range of the Fourier transform spectrometer, making identification of the ion facile. Thus, a reaction was implemented by combining C_{60} and NO_2PF_6 powders in SO_2, a common polar solvent. A similar reaction was also conducted using NO_2SbF_6 . After removing excess NO_2 salt and drying, the powders were studied.

Background information on the structure and symmetry properties of C_{60}, in molecular and solid form, is presented in chapter 2. The sample preparation and experimental techniques are discussed in chapter 3. The results are provided in chapter 4, and a discussion of the findings is given in chapter 5. The conclusions of the study are presented in chapter 6.

Chapter 2

BACKGROUND

2.1 C_{60} Structure

Harry Kroto and co-workers first detected a new species of all-carbon molecules while investigating soot produced by laser vaporization of graphite in a helium atmosphere [Kroto, 1985]. The unusually high abundance in mass spectra, and the apparent stability of the species led to the proposed closed-cage structure . Further experimental and theoretical evidence has indicated that the C_{60} molecule, which appears in greatest abundance, has the geometric structure of a truncated icosahedron. A regular icosahedron, has 20 faces, each an equilateral triangle, with the vertices being formed by the meeting of five of the triangular faces. By cutting off each of the 12 vertices, along a plane perpendicular to the radius, pentagonal faces are created. The structure now consists of 20 hexagons, formed from the original faces, and 12 pentagons. The shape of the truncated icosahedron should be familiar to the sports fan. A regulation soccer ball is stitched together with 12 black pentagons and 20 white hexagons to form a truncated icosahedron. In fact, many of the initial papers referred to the C_{60} molecule as *soccerballene* (or *footballene* in Europe).

In the C_{60} molecule, each vertex of the truncated icosahedron is occupied by a carbon atom. Each atom is bonded to three other atoms along the edges of the solid, structurally resembling the struts and joints in one of Buckminster Fuller's geodesic

domes. Thus, the entire family of closed-caged molecules was dubbed *fullerenes* by Kroto. The most prominent member, C_{60}, was given the name *buckminsterfullerene*, or *buckyball* for short. The crystallite C_{60} solid is called *fullerite*, while the crystallite compounds A_xC_{60} (and offshoots) are called *fullerides*.

Among the fullerenes, the number of hexagons varies widely, from 12 in C_{44} to 260 in C_{540}, but all of the molecules have exactly 12 pentagons. This phenomena was described by Leonhardt Euler, an 18th century mathematician, whose formulas also reveal that the closed cages will only form for an even number of atoms.

2.2 Symmetry and Group Theory

The polyhedral structure of the C_{60} molecule entertains some amazing symmetry properties. Each vertex of the truncated icosahedron lies at the intersection of two hexagon edges and a pentagon edge, so that the vertices of the buckyball are all indistinguishable from one another. The three edges radiating from each vertex (or atom) can also be assigned chemical significance. The hexagon faces have an inner angle of 120° and thus are chemically similar to the six-membered benzene ring, which in some models has alternating single and double bonds. When this simple model is applied to the buckyball, the edges bordering two hexagons are assigned double bonds and the pentagon-hexagon edges are ascribed single bonds. Although more sophisticated models suggest the electrons responsible for the double bonds are delocalized throughout the molecule, the notion of alternating single and double bonds is still notationally convenient.

Two single and one double bond emanate from each vertex. This explains why no symmetry rotations are allowed around an axis passing through a vertex, for that would carry a single bond into a double bond. In fact, only for equal bond lengths are the hexagons regular. A number of spectroscopies have shown that the single and double bond lengths differ slightly (1.46 ± 0.01 Å and 1.40 ± 0.01 Å respectively) [Hedberg, 1991], although the symmetry of the molecule is independent of whether these two lengths are equal.

Consider first the rotational symmetry operators that move vertices of the polyhedron to other vertices. An axis can be drawn so that it passes through the midpoints of two double bonds located directly opposite from one another (Fig.1 (top)). A rotation of 180° about this axis is a symmetry rotation of the molecule. There are 30 double bonds in the molecule, and thus 15 pairs of opposite double bonds. As a result, the icosahedral point group, I, contains 15 elements of twofold rotational symmetry. These elements are denoted C_2 in Schoenflies system for point groups.

Similarly, the midpoints of opposite hexagonal faces can be joined to form an axis for elements with threefold rotational symmetry (Fig. 1 (middle)). Note that these axes have only threefold symmetry, rather than sixfold symmetry, because the single and double bond edges are not equivalent. Including the 120 degree and 240 degree rotation, but not the 360 degree which is equivalent to the identity element, there are 10 x 2 = 20 C_3 elements.

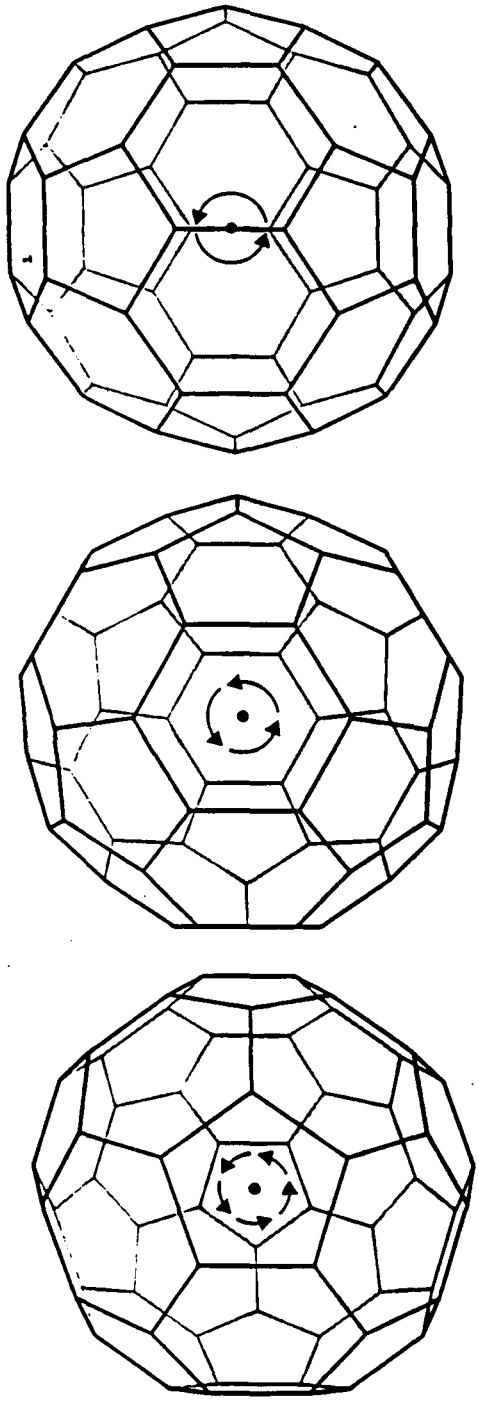

Fig. 1 Rotational symmetries of the buckyball are defined on three sets of axes. There are 15 axes of twofold rotational symmetry (top), 10 threefold axes (middle), and six fivefold axes [Chung, 1993].

There are also six pairs of opposite pentagons in the molecule, creating six axes with fivefold symmetry (Fig. 1 (bottom)). Including rotations by 72, 144, 216 and 288 degrees, but again excluding 360 degree rotations, appends 6 x 4 = 24 C_5 elements.

Including the identity element, E, the total number of symmetry elements accumulated so far is 15+20+24+1 = 60. This classification accounts for all the rotational elements in the point group I. The elements of the full icosahedral group are generated by operating on all the elements of the group I with the inversion operator i, whose effect is to invert all the coordinates of a point and create 60 new improper rotations. This yields a total of 120 operators in the full icosahedral group I_h which is the largest finite symmetry point group in three-dimensional Euclidean space [Chung, 1993].

2.3 The vibrational modes of the C_{60} molecule.

There is rather little literature on normal modes of molecules with icosahedral symmetry because, until recently, there was no physical interest. Having heard of the proposed icosahedrally symmetric buckyball structure, Weeks and Harter (1989) published an extensive vibrational symmetry analysis of icosahedral molecules.

The polyatomic C_{60} molecule has 3N-6 normal vibrational modes (where N = 60). Due to the high symmetry many of these 174 modes are degenerate and only 46 distinct vibrational lines are expected for the isolated molecule. The number of distinct eigenmodes of C_{60} and their degeneracies are presented in Table I. (The label T used here

for the triply degenerate modes are sometimes called F in the literature). Only 14 of the 46 distinct eigenmodes are observable with infrared or Raman spectroscopy.

TABLE I The symmetry group labels, multiplicities, and degeneracies of the eigenmodes of the C_{60} molecule [Weeks *et al.*, 1989]

Parity	I_h group label	Multiplicity	Degeneracy	Activity
	A_g	2	1	Raman
	T_{1g}	3	3	
Even	T_{2g}	4	3	
	G_g	6	4	
	H_g	8	5	Raman
	A_u	1	1	
	T_{1u}	4	3	IR
Odd	T_{2u}	5	3	
	G_u	6	4	
	H_u	7	5	

Four of these 14 eigenfrequencies correspond to the threefold degenerate first-order dipole active T_{1u} modes. The dipole nature of these four infrared active modes can be seen in the stereoscopic representations, presented in Figure 2. In the absence of a central atom and strong radial bonds, the higher frequency normal modes of buckyball (where $T_{1u}(4)$ is the highest) correspond to primarily tangential motion of the carbon atoms. In the three highest frequency modes, the top pentagon is constricted while the bottom pentagon is distended. This distortion, as the atoms alternately crowd toward the

Fig. 2 Stereoscopic views of the T_{1u} modes of the buckyball, beginning with the highest frequency $T_{1u}(4)$ mode. The unperturbed positions of the carbon atoms are shown by open circles.

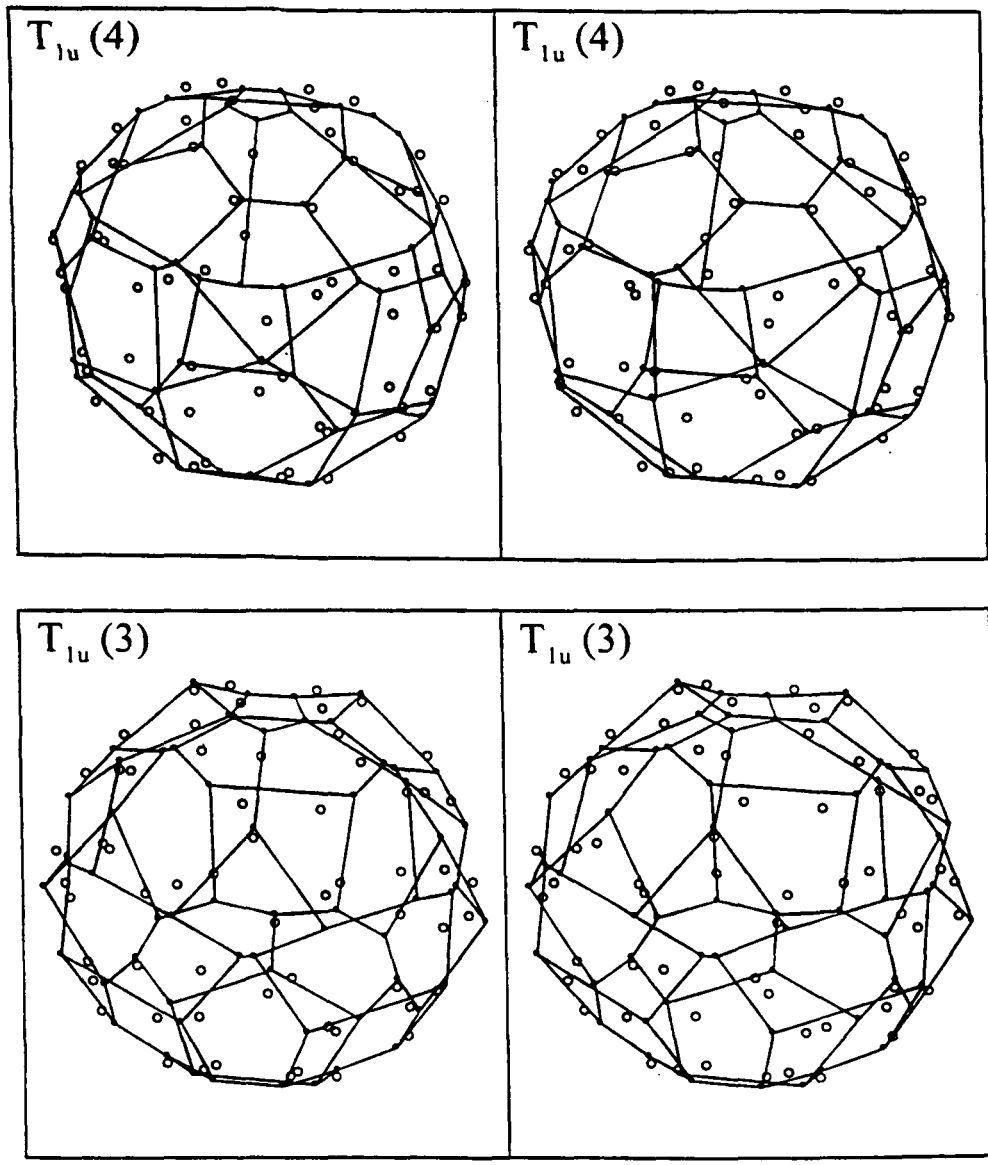

Fig. 2 (continued). Stereoscopic views of the T_{1u} modes of the buckyball [Weeks, 1989].

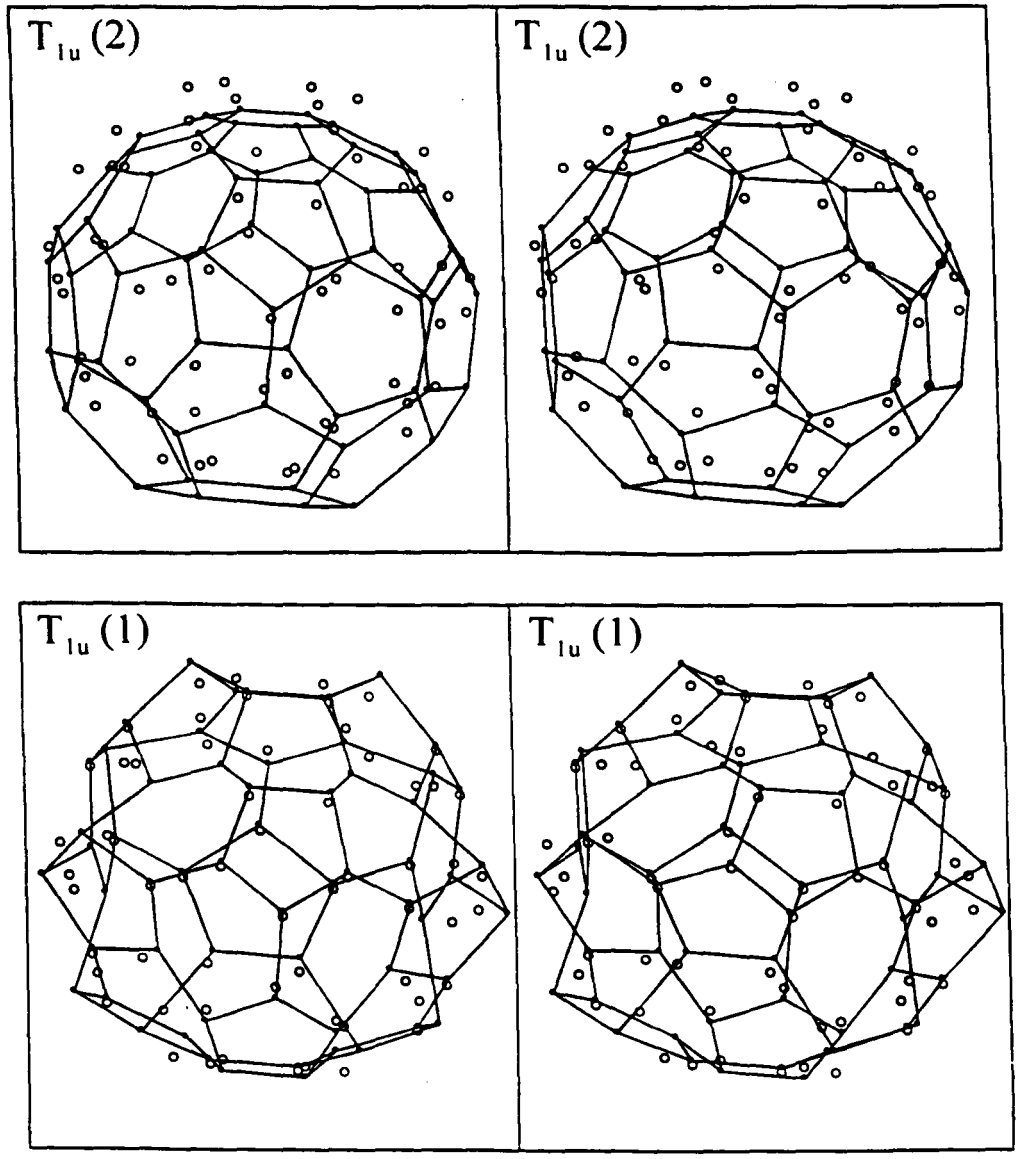

top and then bottom pentagon, shifts charge symmetrically along an axis that passes through the center of the pentagons and defines the dipole axis of the mode. The lowest frequency mode has top and bottom pentagons that remain the same size and move up and down in concert while the remaining nuclei move in the opposite direction. This also has the effect of creating a dipole moment along the axis passing through both pentagons. The remaining two degenerate partners of the four T_{1u} modes generate dipole moments in orthogonal directions [Weeks, 1989].

2.4 C_{60} Solid

In their breakthrough paper, Krätschmer *et al.* (1990) showed that fullerenes could be extracted from condensed carbon soot enabling the preparation of macroscopic quantities of purified C_{60}. X-ray and electron diffraction analysis indicated close packed structures with a nearest neighbour spacing of 10 Å. Their X-ray diffraction pattern of a microcrystaline powder of C_{60} is shown in Figure 3. Subsequent studies have confirmed that the room temperature crystal structure is fcc (O_h^5 / Fm3m space group) with a lattice constant of 14.2Å. But, the symmetry of this space group is based on a point group with a four fold axis. Although the I_h point group of C_{60} contains a large number of symmetry elements, it doesn't contain C_4. Thus, a good fit to the Fm3m X-ray diffraction data was obtained by modelling the C_{60} molecules as spherical shells of charge of radius 3.55Å, implying that the molecules were rotating isotropically with no preferred direction

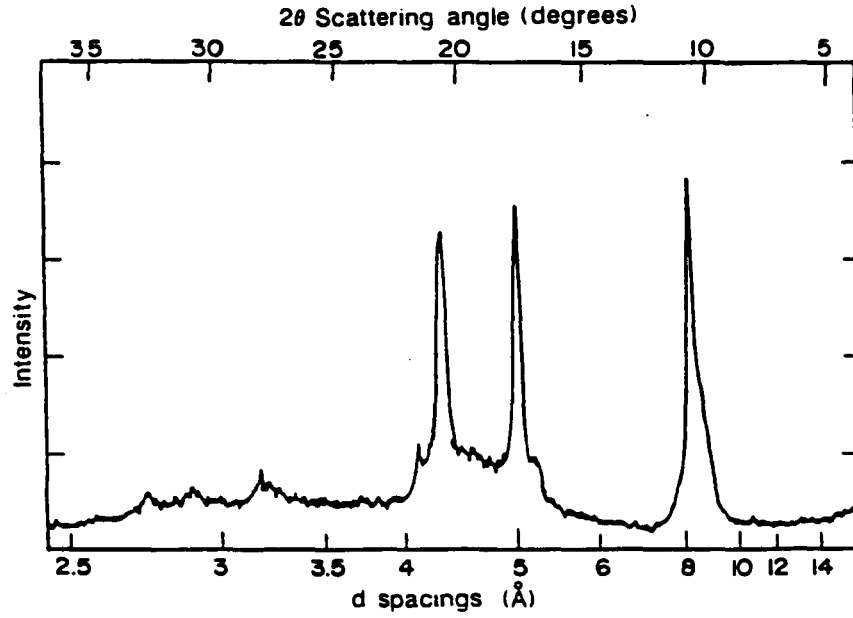

Fig. 3 X-ray diffraction pattern of a microcrystalline powder of C_{60} [Krätschmer, 1990].

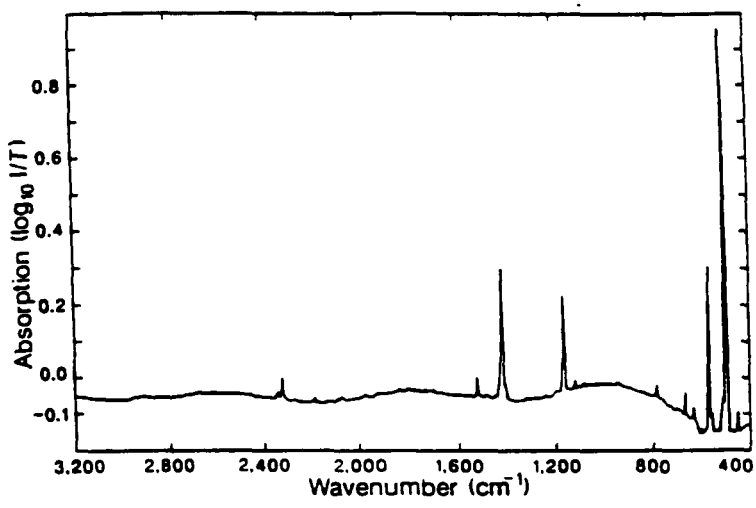

Fig. 4 Infrared absorption spectrum of a coating ~2μm thick of solid C_{60} on a silicon substrate showing four strong bands [Krätschmer, 1990].

[Fischer, 1991]. Further evidence has indicated that the molecules undergo rapid rotational diffusion (~10^{19} Hz) that is nearly isotropic at 300K [Yannonni, 1991].

The high temperature fcc symmetry of C_{60} is lowered to simple cubic (T_h^6 / Pa3 space group) upon cooling below ~250K. The transition results in continued "ratcheting" of the C_{60} molecules between preferred positions in the sc structure [Johnson, 1992]. Below 90K it was found that the molecular motion is essentially quenched [Copley, 1992].

In the paper of Kratschmer *et. al.* one of the key components in the characterization of C_{60} was the appearance of four intense lines in the infrared transmission spectrum, shown in Figure 4 , precisely the number of lines calculated for the molecule. The well expressed absorption peaks indicate the four IR active T_{1u} modes at 528, 577, 1183, 1429. More recent fits to the IR reflectivity from a single crystal have fit the mode frequencies at 527, 576, 1183 and 1428 cm^{-1} [Winkler, 1994]. A number of other weak infrared lines are observed in the IR spectra of C_{60} which were originally attributed to contamination by higher order fullerenes. A study of this fine structure was first reported by Chase *et al.* (1992) and interpreted as contributions from an IR response of I_h forbidden modes or overtones and combination modes. Similar results were observed later by K.A.Wang *et al.* (1993) for thin C_{60} films and by Winkler *et al.* (1994) for single crystal platelets. The authors have tried to correlate the individual peaks to the allowed vibrational modes in the molecule, including some overtones and difference frequencies. This work is cumbersome and the assignments are far from being unique but this, and similar results from Raman scattering, are the only way to have experimental access to all

vibrational modes. Table II presents the measured optically active frequencies in the solid [Bethune, 1991], the values from the fine structure observed in IR specta by K.A.Wang *et al.* (1993) and results from quantum chemical *ab initio* calculations [Quong, 1993].

TABLE II The measured optically active frequencies in the C_{60} solid [Bethune, 1991] are presented and compared to frequencies derived from IR fine structure [K.A. Wang, 1993] and calculated vibrational frequencies [Quong, 1993]. The A_g and H_g modes are Raman active while the four T_{1u} modes are IR active.

Mode	Bethune	Wang	Quong
$A_g(1)$	496	498	478
$A_g(2)$	1458	1470	1499
$T_{1g}(1)$		502	580
$T_{1g}(2)$		976	788
$T_{1g}(3)$		1358	1252
$T_{2g}(1)$		567	548
$T_{2g}(2)$		865	610
$T_{2g}(3)$		914	770
$T_{2g}(4)$		1360	1316
$G_g(1)$		486	486
$G_g(2)$		621	571
$G_g(3)$		806	759
$G_g(4)$		1076	1087
$G_g(5)$		1356	1297
$G_g(6)$		1525	1505
$H_g(1)$	273	273	258
$H_g(2)$	437	433	439
$H_g(3)$	710	711	727
$H_g(4)$	774	775	767

TABLE II (continued)

Mode	Bethune	Wang	Quong
$H_g(5)$	1099	1101	1193
$H_g(6)$	1250	1251	1244
$H_g(7)$	1428	1427	1444
$H_g(8)$	1575	1578	1576
$A_u(1)$		1143	850
$T_{1u}(1)$	527	527	547
$T_{1u}(2)$	577	576	570
$T_{1u}(3)$	1183	1183	1176
$T_{1u}(4)$	1428	1429	1461
$T_{2u}(1)$		356	342
$T_{2u}(2)$		680	738
$T_{2u}(3)$		1026	963
$T_{2u}(4)$		1201	1185
$T_{2u}(5)$		1577	1539
$G_u(1)$		400	357
$G_u(2)$		760	683
$G_u(3)$		924	742
$G_u(4)$		970	957
$G_u(5)$		1310	1298
$G_u(6)$		1446	1440
$H_u(1)$		343	404
$H_u(2)$		563	539
$H_u(3)$		696	657
$H_u(4)$		801	737
$H_u(5)$		1117	1205
$H_u(6)$		1385	1320
$H_u(7)$		1559	1565

A review summarizing the status of the application of IR spectroscopy to the field of fullerene science, concentrating primarily on pristine and alkali metal doped C_{60}, is presented by Kuzmany *et al.* [1995]. In terms of other relevent solid state properties, the intermolecular bonds in the fcc lattice of C_{60} are largely van der Waals in nature, while the intramolecular bonds are covalent. The molecular solid C_{60} is an electrical insulator with a sizable gap, 1.8 eV [Reber, 1991].

2.5 C_{60} Compounds

The fullerides exhibit a wide range of interesting properties, and one of the most alluring is the diversity of their interactions with other species. The electron affinity of neutral C_{60} has been determined experimentally to be $A(C_{60})$=2.65 eV [L. Wang, 1991], only slightly smaller than that of the electronegative elements in group VII A, which makes the molecule a good electron acceptor. In the alkali metal fullerenes, denoted A_xC_{60}, the doping level is exceptionally high, with values reaching x=6 for K-, Rb, Cs-C_{60}, and x=10 for Na-C_{60}. These materials exhibit almost complete charge transfer, at least for $x \leq 6$, with the fullerene molecule becoming C_{60}^{6-} in the solid state. Furthermore, the A_3C_{60} phases of the alkali metal doped fullerenes are metallic and display superconductivity with transition temperatures as high as 33K (for $Rb_1Cs_2C_{60}$) [Tanigaki, 1991].

On the other hand, the relatively low ionization potential of the C_{60} molecule, determined experimentally to be $I(C_{60})$=7.6 eV [Yoo, 1992], lies close to that of

electropositive Mg, making the molecule a good electron donor as well. Even so, there have been few reported studies of the intercalation of acceptors in C_{60}.

A reaction between AsF_5 gas, dissolved in SO_2, and C_{60} powder was first reported in 1994 [Datars, 1994]. Cu K_α X-ray powder pattern (Fig. 5) of the compound identified the structure as body-centered-tetragonal (bct) with lattice parameters of a=12.794Å and c=12.426Å, distinctly different than pristine C_{60}. The observed and calculated X-ray diffraction angles for the tetragonal lattice are presented in Table III. The NMR ^{19}F spectrum of the AsF_5 reacted compound showed a quartet very similar to the quartet in $NaAsF_6$. Mass analysis of the sample indicated that the integrity of the buckyball was maintained with the characteristic multiplit appearing at 720 a.u. The presence of AsF_x^- (x=0,1,2,3 and 4) ions were also observed in the mass spectra. On comparison with $Hg_3(AsF_6)_2$, a strong absorption in the infrared spectrum at 702 cm^{-1} was assigned to the presence of AsF_6^- in the sample [Datars, 1995]. Combined with the absence of lines due to gaseous AsF_5 in the spectra, this led to the proposed composition of $C_{60}(AsF_6)_x$. Yet, even with this compelling evidence, the existence of this compound was called into question due to the poorly resolved C_{60} lines in the IR spectrum. The sealed cell used to contain the air sensitive sample between KBr windows was hindered by low transmission. The 525 and 575 lines of C_{60} appeared weak and unshifted, while the higher frequncy modes were not observed or were obscured by a number of lines attributed to impurities on the windows.

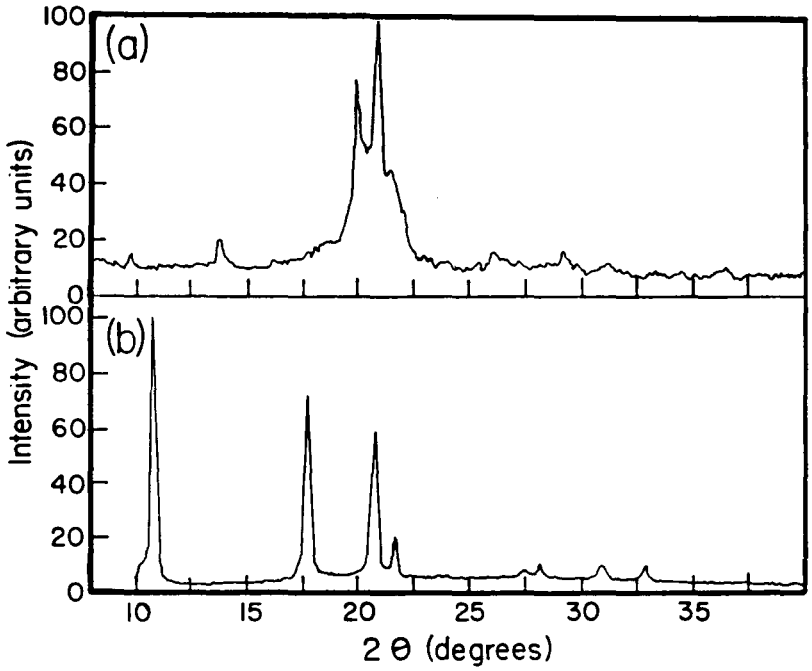

Fig. 5 X-ray diffraction with Cu K_α radiation of (a) C_{60} powder reacted with AsF_5, (b) C_{60} [Datars, 1994].

Table III Observed X-ray diffraction angles of the C_{60} powder reacted with AsF_5 and calculated values for a tetragonal lattice with a=12.794Å and c=12.426Å.

h	*k*	*l*	$2\theta_{obs}$	$2\theta_{calc}$
1	1	0	9.783	9.769
2	0	0	13.769	13.832
2	0	2	19.933	19.906
2	2	1	20.851	20.883
0	0	3	21.466	21.436
3	2	1	26.122	26.095
2	2	3	29.178	29.212
4	2	0	31.240	31.144

Chapter 3

EXPERIMENTAL DETAILS

3.1 Material synthesis

With the proposed composition of $C_{60}(AsF_6)_x$ for the AsF_5 reacted compound, two subsequent preparations using larger amounts of material were performed by Dr. P. Ummat, and led to a determination of x=1.9 by weighing the final powder [Datars, 1995].

The diffusion of dopants within crystallites of solid C_{60} is much slower than previously found in graphite intercalation compounds. This behaviour is due to the fact that the dopant ions in C_{60} must hop between well-seperated hole sites in the lattice versus simple two-dimensional diffusion through interlayer regions in graphite. Thus, a solid-solution method of AsF_5 gas, dissolved in SO_2, reacted with C_{60} powder was utilized in order to prepare a homogenous compound. The dark brown C_{60} powder was observed changing to a green coloured suspension after a few hours, with the complete reaction taking place, with continuous stirring, over several days. The excess SO_2 and AsF_5 were decanted and condensed leaving a dried powder with a uniform dark green colour. The reaction of AsF_5 forms AsF_6^- through the reaction

$$3AsF_5 + 2e^- \rightarrow 2AsF_6^- + AsF_3$$

which has been established for the formation of $Hg_3(AsF_6)_2$ [Davies, 1971]. Here, the AsF_5 oxidizes C_{60} to form AsF_6^- and to maintain charge neutrality of the compound, as the transparent AsF_3 liquid is decanted with the SO_2. Exposing part of the sample to room

atmosphere indicated air sensitivity, as it changed to a brown colour. Thus, all handling of the sample was conducted in an argon dry box.

The process of synthesizing the phosphorous and antimony hexafluoride fullerides was conducted in a slightly different manner than for the arsenic hexafluoride compound. PF_5 is a colourless gas which reacts immediatly with water, thus any moisture would generate HF. It is also a weaker Lewis acid than AsF_5. Thus, for ease and safety of handling, and to initiate a reasonable reaction time, the hexafluoride salt, NO_2PF_6, was employed as a direct source of PF_6^- ions. In the glove box, 500 mg of C_{60} was combined with a stoichiometric amount of NO_2PF_6 (using a 1:2 ratio as suggested by $C_{60}(AsF_6)_{1.9}$). The powders were thoroughly mixed using a mortar and pestle and transferred to a Pyrex H-shaped reaction vessel (Fig. 6). Prior to this, all utensils and the reaction vessel were heat treated to remove any moisture. The mixture was deposited in side A of the double ampoule reaction vessel via the attached tubing B, which was subsequently sealed. With the valve to neck C closed, the vessel was removed from the argon dry box and fastened to the vacuum line. The vessel was evacuated before SO_2 gas, introduced into the vacuum line, was condensed into ampoule D using a liquid nitrogen bath. The necks, B and C, were permanently sealed using a natural gas torch. As the white solid SO_2 warmed to a clear liquid it was poured into side A of the reaction vessel. With valve E closed, the brown powder in suspension was agitated for two weeks using the magnetic stir bar. Afterwards the SO_2, decanted through filter F back to ampoule D, had a distinctive brown tinge indicative of dissolved NO_2. Ampoule A was gently cooled, condensing

Fig. 6 The H-shaped reaction vessel, used in the sample preparations, connects two ampoules via pyrex tubing, a valve and a paper filter.

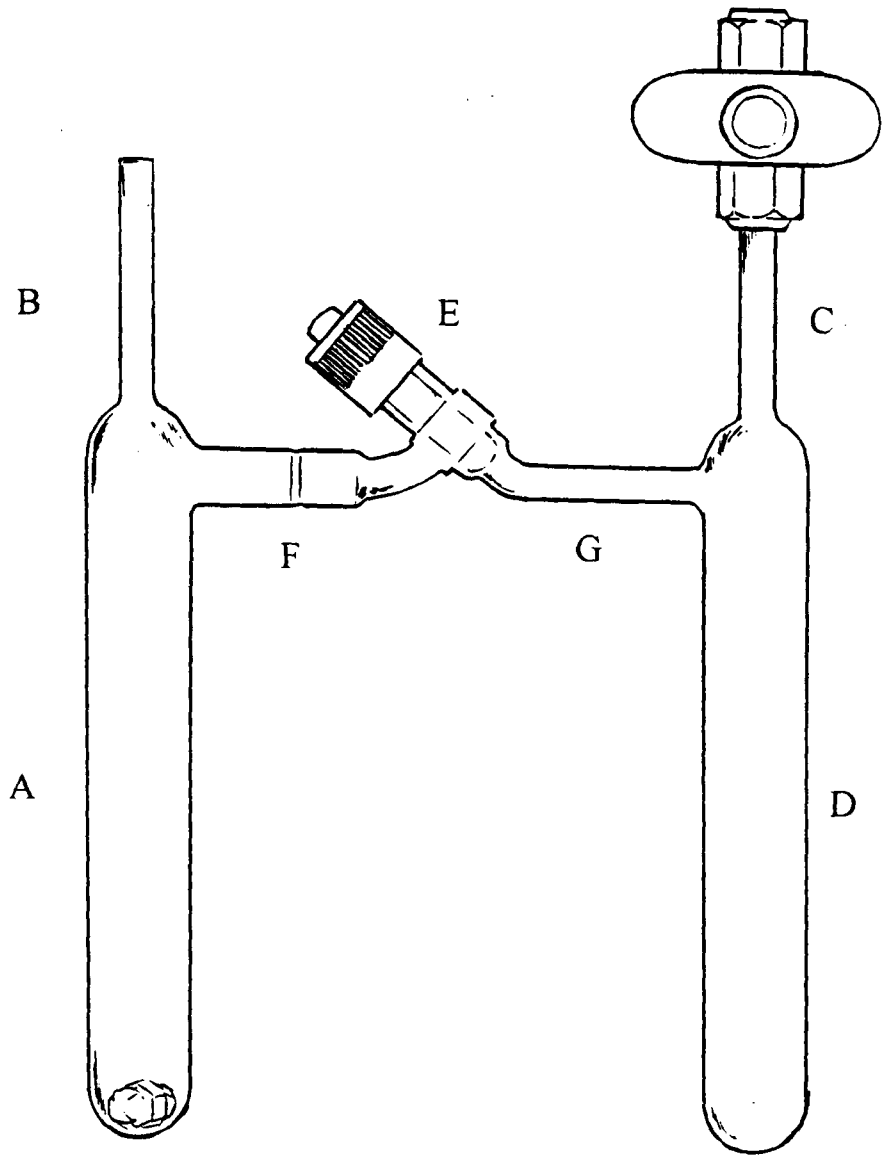

liquid SO_2 back into the ampoule containing the powder then subsequently decanted back into ampoule D. This was repeated a number of times to remove excess NO_2PF_6 salt from the powder mixture. Ampoule D was then immersed in liquid nitrogen to condense the SO_2 to a solid and completely dry the powder. The sample was then removed in an inert atmosphere for study. A reaction using NO_2SbF_6 was performed in an identical manner, with a similar brown colour observed in the liquid SO_2.

3.2 The Fourier Transform Spectrometer

In the Michelson interferometer, light from the source strikes a thin, partially reflecting beam splitter and is divided into two beams that are returned by mirrors and recombined at the beam splitter. The intensity of the recombined and interfering beams, recorded as a function of the optical path difference as one mirror is moved, yields an interferogram. The desired spectrum, the source intensity as a function of wavenumber, can be recovered from the recombined beams by Fourier transform analysis. This same idea, but using a sample in the beam path of a broad band infrared source, is used in the Fourier transform spectrometer (FTS).

The Bio-Rad FTS-40 system uses a ceramic source which emits IR useful energy from 5000 to 80 cm^{-1}. Figure 7 shows the optical path (shaded) of the broad band IR radiation which is collected by an ellipsoidal mirror, M1, and refocused at an aperture (not shown). An off-axis paraboloid, M2, collects the IR radiation and produces a colimated beam which is directed onto the Mylar beamsplitter. The collimated, modulated beam

Fig. 7 Optical beam path in the Bio-Rad Fourier transform spectrometer.

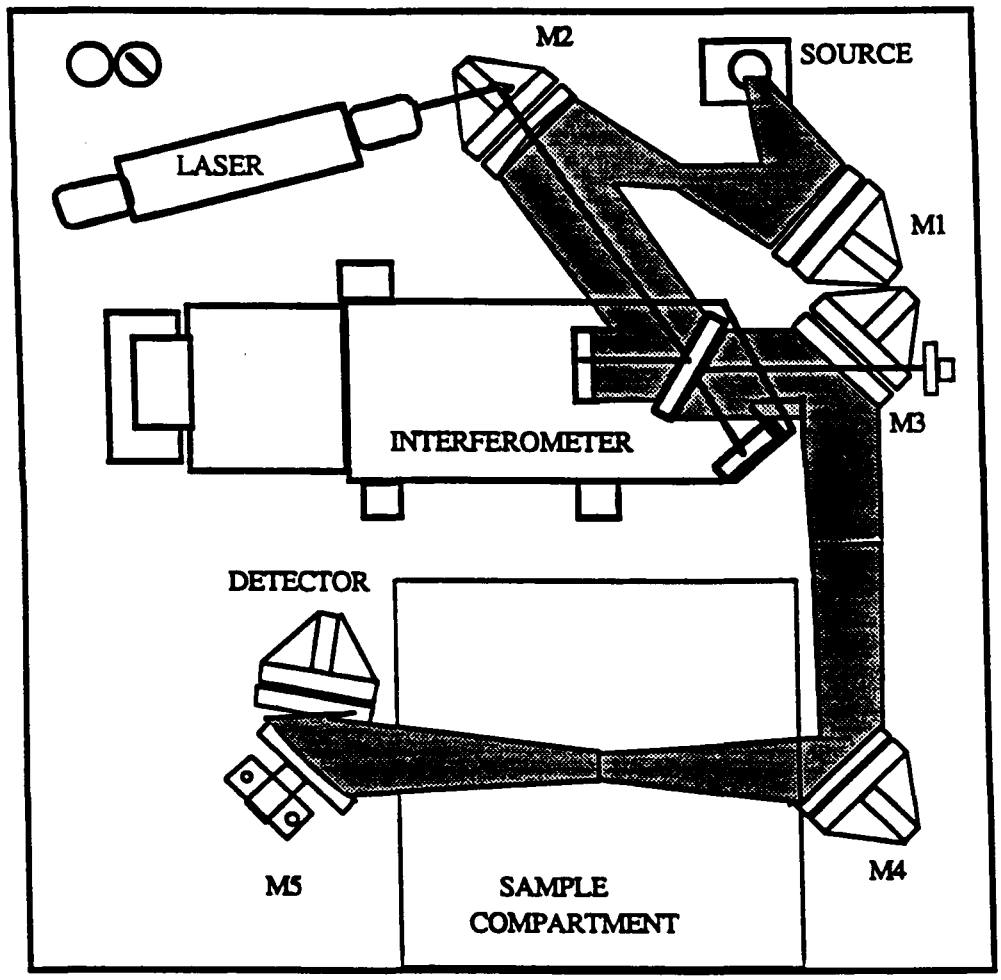

exits from the interferometer, is reflected by a flat mirror M3, and collected by an off-axis paraboloid M4 which focuses the beam down to a 12 mm circular image in the middle of the sample compartment. The beam then travels to an aspheric mirror M5 which focuses the beam to a 2mm image on the detector (composed of deuterated tryglycine sulfate).

A key component of the Fourier transform spectrometer is that the mirror movement is monitored to high precision with a monochromatic HeNe laser, so that the wavenumber scale of the transformed spectrum is highly accurate. The laser optical path enters coaxially into the IR beam at M2, is split by a small diameter beamsplitter centered on the IR beamsplitter, recombines and the modulated beam exits the IR beam through M3, where it is directed to a silicon photodiode (Bio-Rad users manual). In this configuration the FTS-40 operates from 4000 to 400 cm^{-1} with a resolution of $2cm^{-1}$.

The sample material was combined with potassium bromide (Aldrich, FT-IR grade 99+%) using a mortar and pestle, then pressed into a pellet using a stainless steel pellet press. All samples were treated as air sensitive and were handled in an argon glove box. Transportation of the pellet from the glove box to the FTS sample chamber was performed via a sealed cell (Fig. 8). The sample was surrounded by a stainless steel cylinder sealed to the base with a rubber O-ring. The plexiglass plate allowed the sample holder to be sealed to the FTS compartment.

Due to strong infrared absorption by water vapour and carbon dioxide the sample compartment was purged with dry nitrogen prior to background scans (empty sample

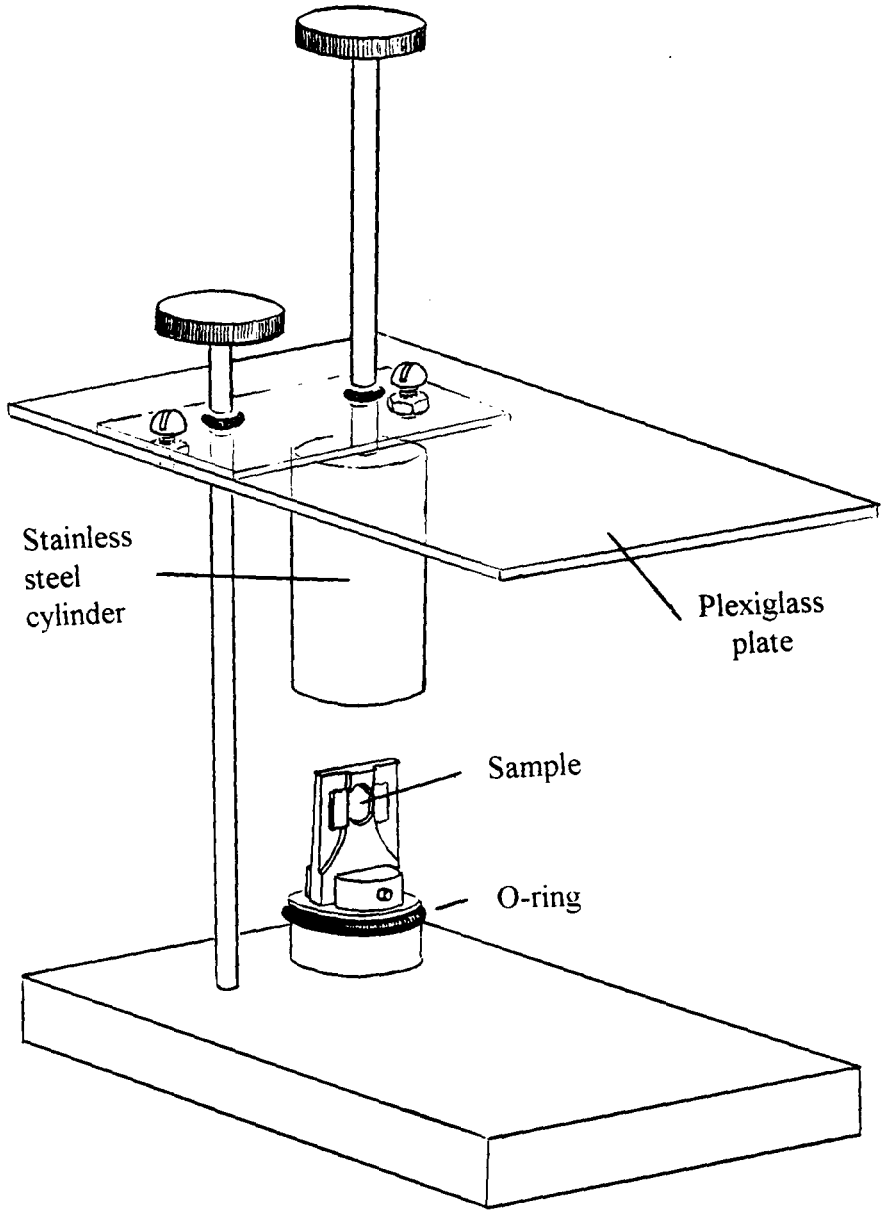

Fig. 8 The apparatus used for transporting the air sensitive sample to the FTS chamber. Notches in the base permitted proper allignment and the plexiglass plate allowed the lower portion of the apparatus to be sealed in the FTS sample compartment.

chamber) and sample scans. Using an external shaft the stainless steel cylinder was lifted away from the base exposing the sample to the IR beam.

3.3 Heat treatment

Thermal decalation of the samples was conducted with the powder contained in a Pyrex reaction vessel (which was previously heat treated under vacuum to remove moisture). The reaction vessel had a neck of 6mm (outer diameter) Pyrex tubing to which a teflon adaptor and valve were connected to facilitate attatchment to a vacuum line. The reaction vessel, containing the powder sample, was sealed from the environment during transit between the argon dry box and the vacuum line. The pressure in the line was reduced to 7 mTorr using a roughing pump and liquid nitrogen cold trap. Moisture condensed on the inner walls of the vacuum line was driven off by heating with a natural gas Bunsen burner. The valve, connecting the reaction vessel to the vacuum line, was opened very slowly in order to minimize the loss of sample. The reaction vessel was heated using a vertical furnace controlled by a LOVE temperature controller with feedback provided by a type K thermocouple. After 30 minutes, the oven was removed to allow the sample to cool to room temperature. The reaction vessel was then sealed and transported back to the argon dry box in preparation for IR measurement.

3.4 X-ray techniques

Powder samples were positioned on a glass plate in a brass sample holder specifically constructed for air sensitive samples. The window of the cell was plastic wrap, sealed tightly with a rubber O-ring. The crystal structures of the samples were observed using Cu-K_α x-ray diffraction data taken by W. Gong of the Brockhouse Institute for Materials Research.

3.5 Resistivity measurements

The sample material was pressed into pellets and cut into thin rectangular slabs (approximately 6 x 4 x 0.5 mm). Electrical contacts were mounted to the sample using silver paste in a four terminal configuration (Fig. 9(inset)). The current leads had a large diameter but the voltage leads, carrying negligible current, were fashioned as small as possible. The use of silver paste was justified by the absence of a resistance change in the sample after applying the contacts, ensuring that the solvent did not affect the electronic properties.

The pressed powder sample, mounted on Pyrex, was secured to a platform constructed of Kel-F, a high resistance plastic. The platform housed both a carbon-glass resistor (CGR) and a platinum resistor calibrated for temperature measurements. Prior to removal from the inert argon atmosphere of the dry box the probe was sealed using a stainless steel can and a ring of indium wire (Fig. 9).

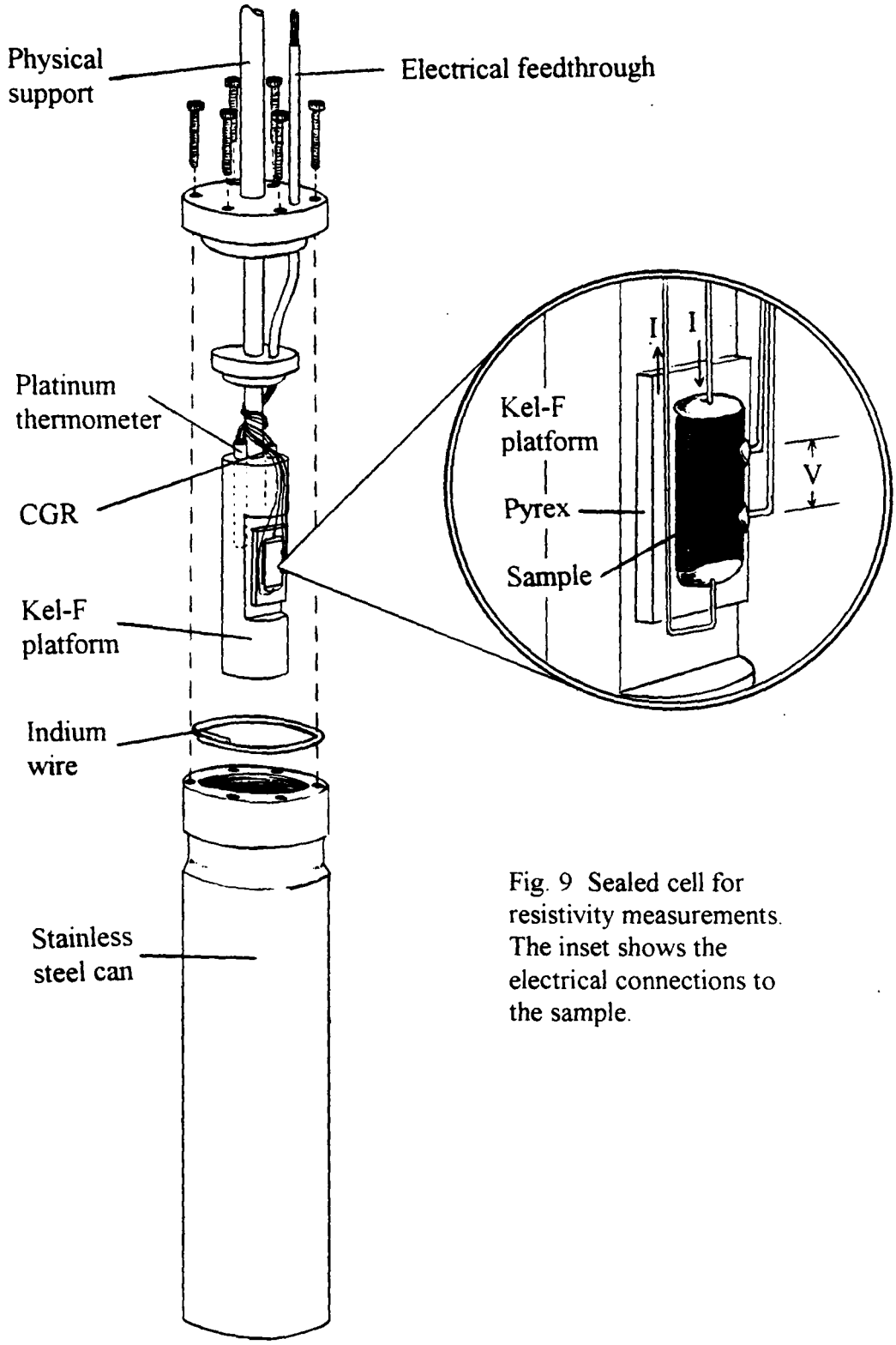

Fig. 9 Sealed cell for resistivity measurements. The inset shows the electrical connections to the sample.

The probe head was physically mounted to a measuring probe and electrical connections were made using pin connectors from the probe head feedthroughs. Current was supplied to the sample by a Keithley 224 programmable current source and monitored using a known reference resistance held at a fixed temperature in a liquid nitrogen bath.

In the case of many semiconducting samples the contact between metallic lead wire and semiconductor is partially rectifying (having low resistance to current flow in one direction and higher resistance in the opposite direction). The voltage drop across such a junction when a current is forced through it in the "back" direction can be larger than the regular voltage across the sample. In a four wire method using a high impedance detector the contact voltages from rectifying contacts in the voltage leads circuit are greatly reduced, since little current flows in this circuit at the moment of measurement. Also, with high resistance materials, electrons may not pass freely in and out of the sample creating spurious voltages at the contacts. Usually these spurious voltages reverse sign for reversal of current flow and can be overcome by taking reading with current flowing in both directions and averaging [Subbarao, p.261]. Thus, the voltage leads from the sample were first connected to a lab constructed high impedance amplifier with an input impedance of 6 GΩ. The signal was then passed to a Keithley 181 nanovoltmeter with the output taken directly to a 286 personal computer. The current direction was switched using a Hewlett-Packard 59306A relay actuator. The CGR and platinum thermometer currents were supplied by separate DC power supplies. The sample current and

thermometer currents and voltages were fed to a Keithley 705 scanner and relayed to both the 286 PC and a Hewlett-Packard 3478A multimeter for display.

The PC controlled the data acquisition and calculated the CGR and platinum thermometer temperatures and the sample resistance, and all readings were averaged with respect to sample current direction. In order to perform temperature dependent studies nitrogen was transferred to an outer cryogenics dewar surrounding the probe. The use of the outer dewar avoided direct contact of the nitrogen and the probe head, slowing the rate of temperature change and minimizing any temperature gradients between the sample and thermometers.

Chapter 4

EXPERIMENTAL RESULTS

4.1 Infrared and X-ray analysis of $C_{60}(AsF_6)_{1.9}$

The Fourier transform infrared spectrum of the $C_{60}(AsF_6)_{1.9}$ powder is shown in Figure 10, over the range 4000 to 400 cm^{-1}, revealing a number of features. Note the large broad absorption centered at 703 cm^{-1} which is assigned to the ν_3 vibration of the AsF_6^- ion, reported at 700 cm^{-1} [Naulin, 1976]. The $T_{1u}(1)$ and $T_{1u}(2)$ modes of C_{60}, at 527 and 577 cm^{-1}, are unshifted in frequency. The $T_{1u}(3)$ mode of C_{60}, at 1183 cm^{-1}, appears somewhat obscured by higher frequency counterparts. There are three strong peaks, similar in intensity and width, at 1549, 1405 and 1322 cm^{-1}, near the unobserved $T_{1u}(4)$ line of pristine C_{60} at 1428 cm^{-1}.

Successive heat treatment of the sample was performed in vacuum at different temperatures in an attempt to decalate the sample and aid in identification of the modes. Heat treatments up to 150°C resulted in little change in the infrared spectrum of the $C_{60}(AsF_6)_{1.9}$. However, progressive treatments up to 350°C resulted in a decrease in the intensity of the 703 cm^{-1} line and an increase in the relative strength of the C_{60} lines at 527 and 576 cm^{-1} (Fig. 11). The decrease in intensity of the three lines, at 1549, 1405 and 1322 cm^{-1}, and the emergence of the absorption at 1429 cm^{-1} with heating (Fig. 12), suggests that the triplet may be due to symmetry breaking of the triply degenerate $T_{1u}(4)$ mode. The emergence of sharply defined absorption lines at 527, 576, 1183 and 1429

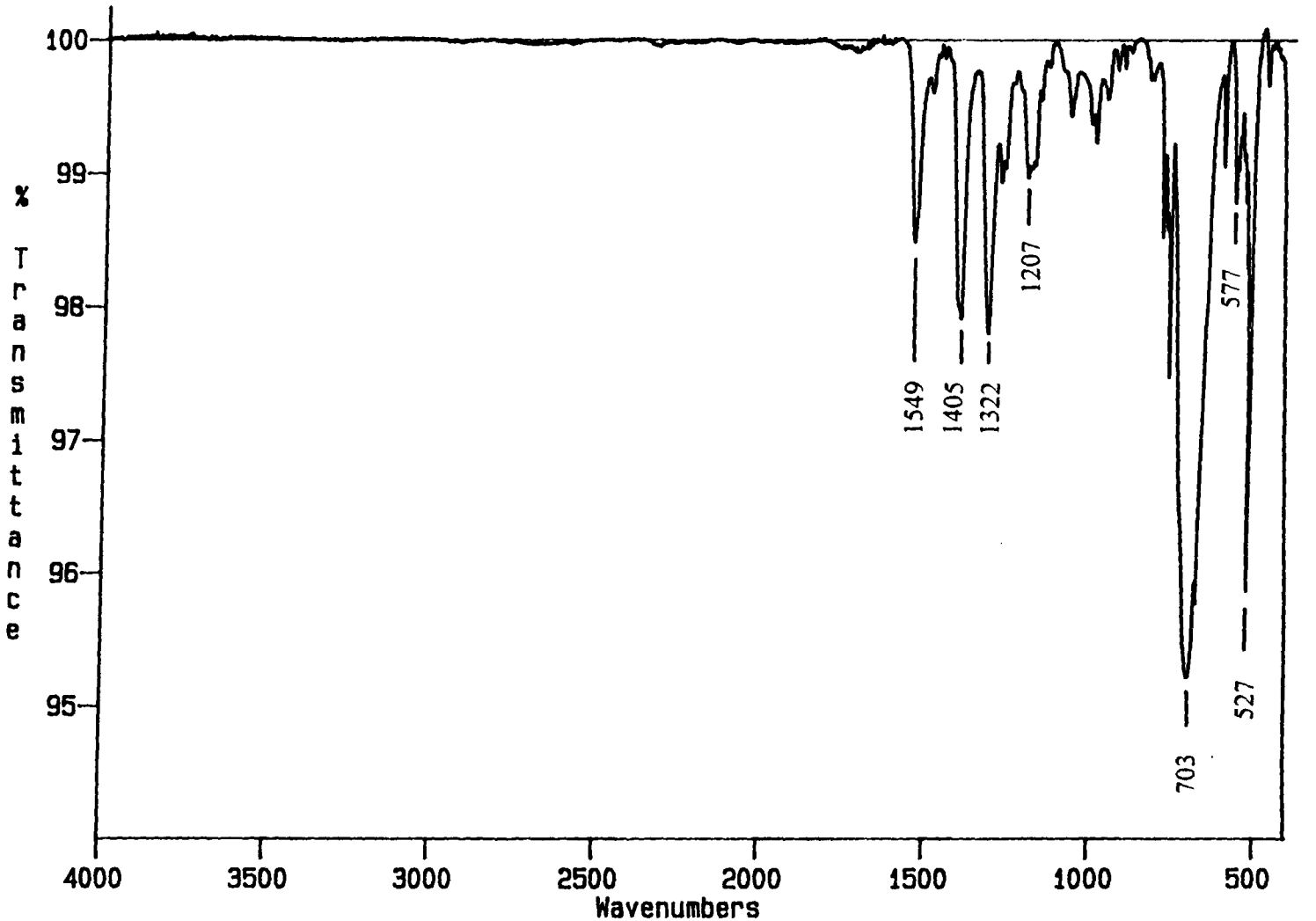

Fig. 10 The Fourier transform infrared spectrum of $C_{60}(AsF_6)_{1.9}$.

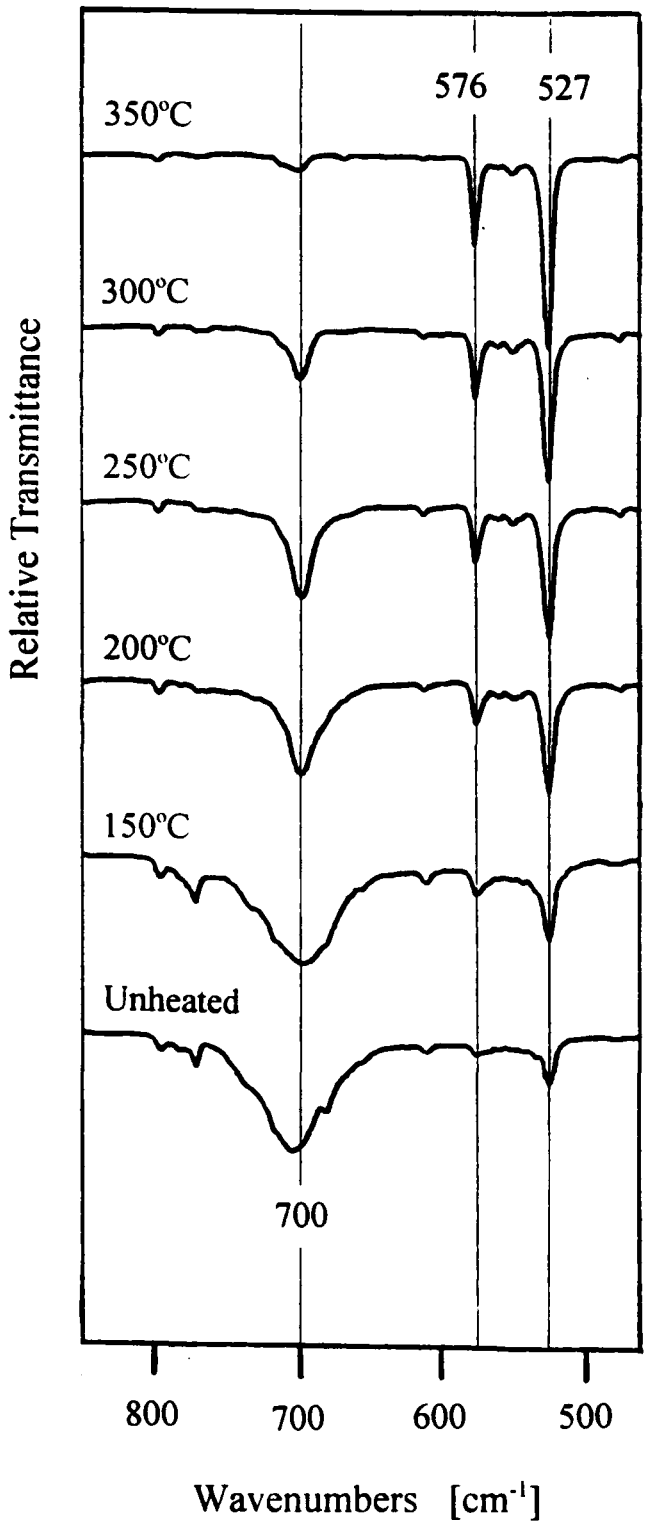

Fig. 11 Succesive heat treatments of the sample led to a decrease in the AsF_6^- absorption, near 700 cm^{-1}, and the increase of the relative strength of the C_{60} lines in the IR spectra.

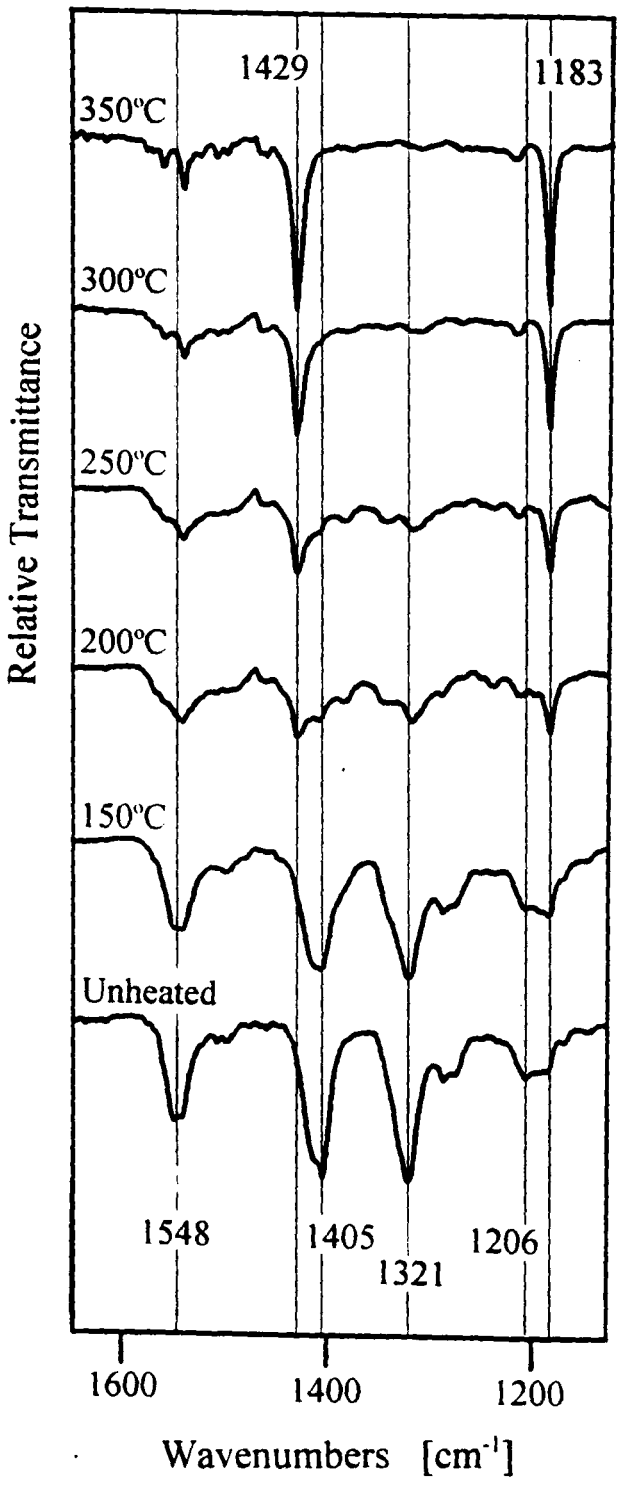

Fig. 12 The 1405 cm^{-1} line shifts to 1429 cm^{-1} with increased heating, as the proposed triplet fades away. The emergence of the 1183 cm^{-1} line also indicates the return of undoped C_{60}.

cm^{-1} inferred that the sample was reverting back to the initial C_{60} starting material. These four strong C_{60} lines indicated that the buckyballs stayed intact during the intercalation and decalation of the sample.

The successful decalation of the $C_{60}(AsF_6)_{1.9}$ sample was supported by X-ray diffraction analysis which showed the return of the fcc C_{60} lattice structure after heat treatment. Fig. 13 (a) shows the X-ray diffraction pattern of the arsenic hexafluoride fulleride which was indexed as body-centered tetragonal (Datars, 1994). The X-ray powder pattern of the sample heated to 350°C for 30 minutes in vacuum, then cooled to room temperature, is presented in Fig 13 (b). Although the diffraction lines are broad, due to small grain size and incomplete decalation, they are clearly observed at 2θ angles of 10.8, 17.9 and 20.8, the position of the three strongest lines in the pristine C_{60} pattern.

4.2 C_{60} powder reacted with NO_2PF_6

The infrared spectrum of the C_{60} powder reacted with NO_2PF_6 in liquid SO_2 is shown in Figure 14. The high frequency portion of the spectrum is completely bare. The low frequency portion has quite a number of absorption regions, and is shown expanded in Figure 15. The broad ν_3 absorption of PF_6^-, reported by Begun and Rutenberg (1967) at 830 cm^{-1}, is observed as well as the sharp ν_4 mode reported at 558 cm^{-1} (seen here at 559 cm^{-1}). The C_{60} lines in the spectrum appear unshifted, but the $T_{1u}(4)$ line is flanked by two neighbouring absorptions, at 1538 and 1334 cm^{-1}, that are close in frequency to the observed lines, at 1549 and 1322 cm^{-1}, in $(AsF_6)_{1.9}C_{60}$. The X-ray diffraction pattern

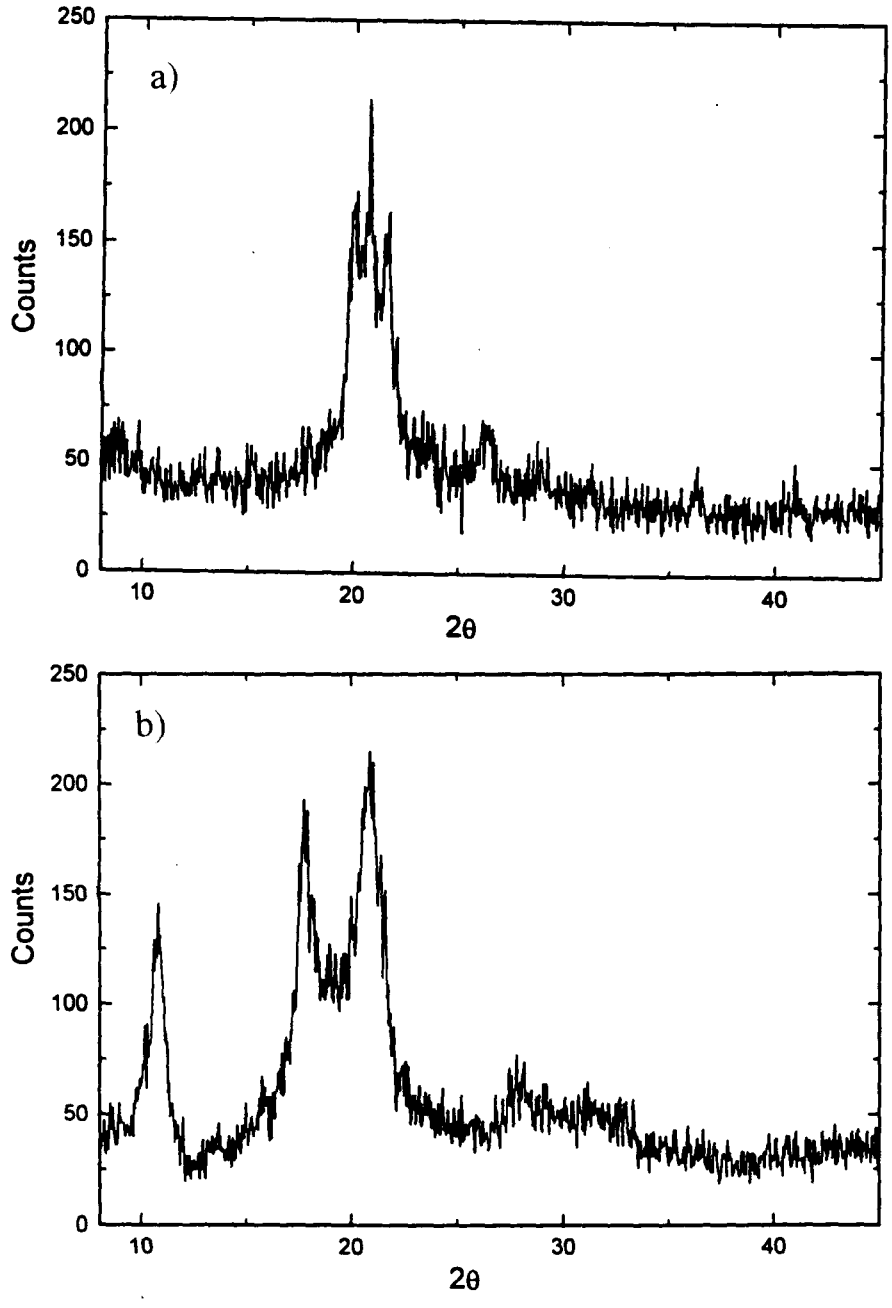

Fig. 13 X-ray diffraction pattern of (a) $C_{60}(AsF_6)_{1.9}$ (b) $C_{60}(AsF_6)_{1.9}$ heated at 350°C showing the return of the C_{60} pattern.

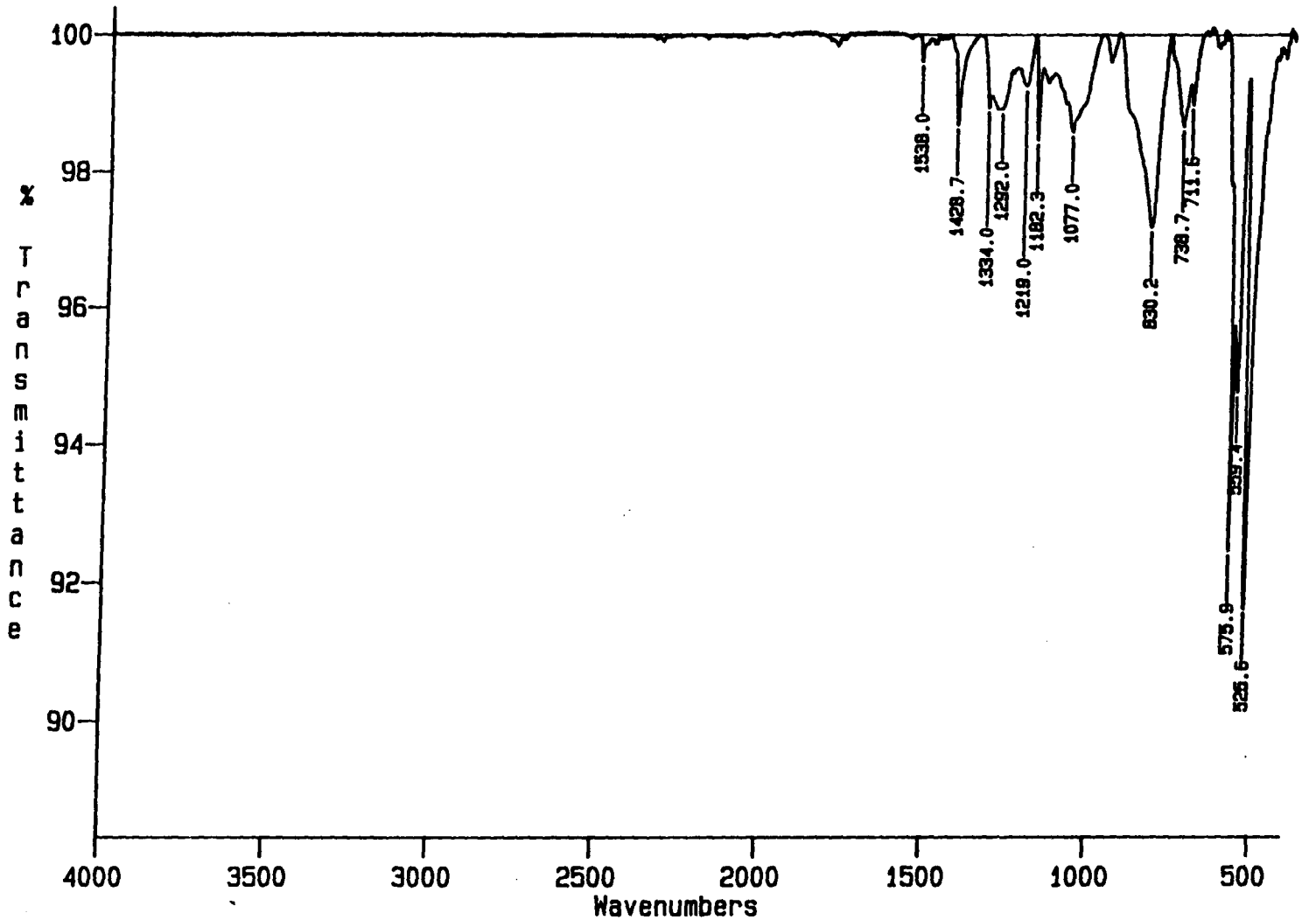

Fig. 14 Infrared spectra of C_{60} powder reacted with NO_2PF_6

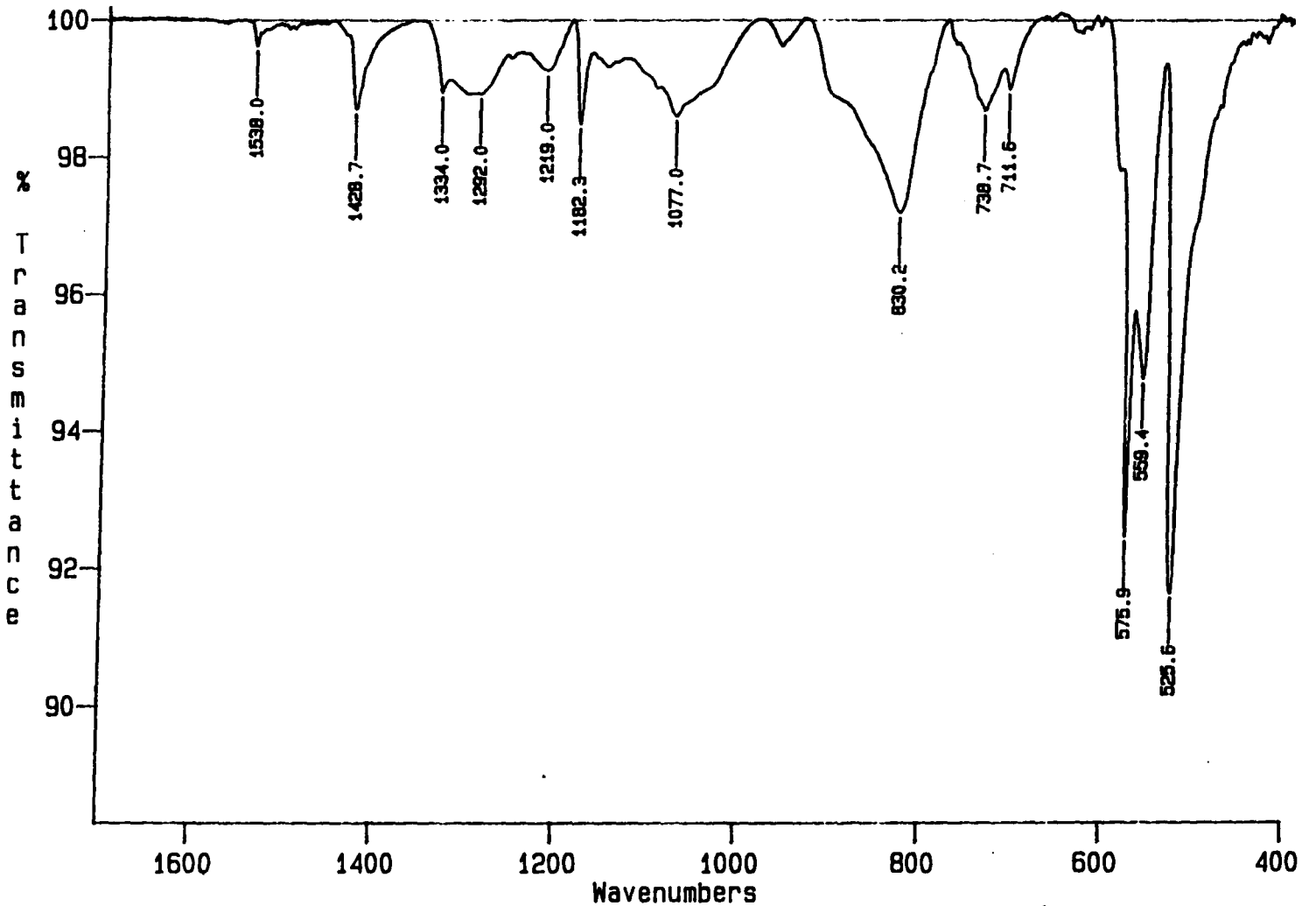

Fig. 15 Infrared spectra of C_{60} powder reacted with NO_2PF_6 (400-1700 cm^{-1}) showing the broad ν_3 and the sharp ν_4 absorption, at 830 cm^{-1} and 559 cm^{-1} respectively, of the octahedral PF_6^- ion.

showed no shift in the 2θ values, as compared to pristine C_{60}, although it did show changes in the relative intensity of the lines. Heat treatment of the PF_6^- compound at 350°C under vacuum yielded an IR spectrum that was close to that of pristine C_{60} (Fig. 16).

4.3 C_{60} powder reacted with NO_2SbF_6

The infrared spectrum of the C_{60} powder reacted with NO_2SbF_6 is shown in Figure 17. The strong broad absorption of SbF_6^- at 660 cm^{-1} is clearly visible, and lies very close (for such a broad peak) to the reported value of 669 cm^{-1} (Begun, 1967). The C_{60} peaks are unshifted, but again there are similarities with the previous spectra. The inset of Figure 16 shows the region surrounding the $T_{1u}(3)$ and $T_{1u}(4)$ lines. The $T_{1u}(3)$ line, at 1182, has a higher frequency counterpart at 1226, and the $T_{1u}(4)$ line is flanked by absorptions at 1538 and 1334cm^{-1}, again close to the strong absorptions at 1549 and 1322 cm^{-1} observed in $(AsF_6)_{1.9}C_{60}$. The x-ray diffraction pattern of the powder shows lines other than those of C_{60}, but these have not been indexed. The IR spectra of the sample, after heat treatment at 350°C, revealed only the four strong absorption lines of pristine C_{60} indicating that the sample had been decalated.

4.4 Resistivity measurements

A typical curve of the resistance of a $C_{60}(AsF_6)_{1.9}$ sample as a function of temperature is presented in Figure 18. The semiconducting character of the sample,

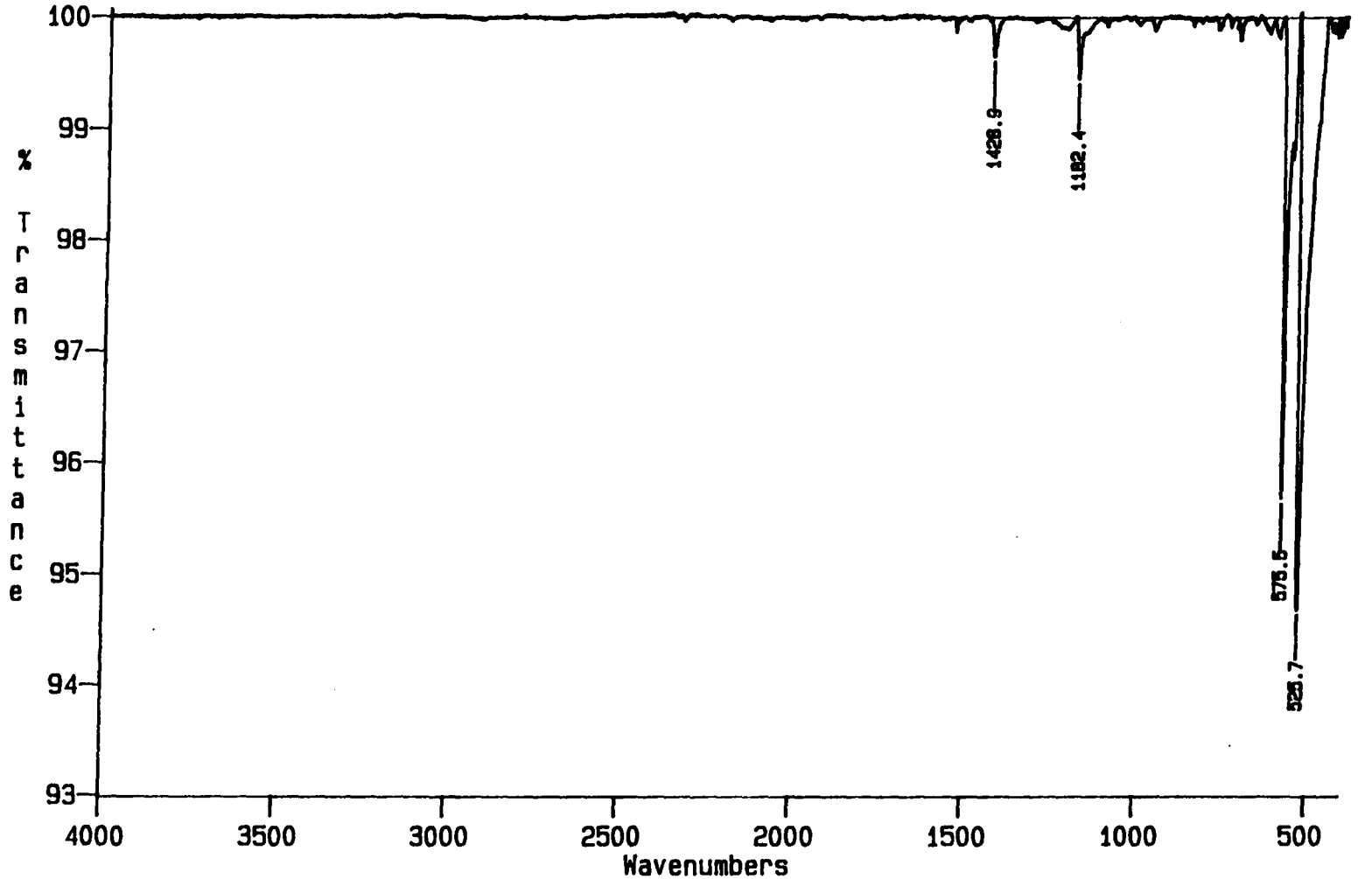

Fig. 16 The IR spectra of C_{60} powder reacted with NO_2PF_6 after heating at 350°C shows the four strong C_{60} lines and the decrease of other absorptions observed in the unheated powder.

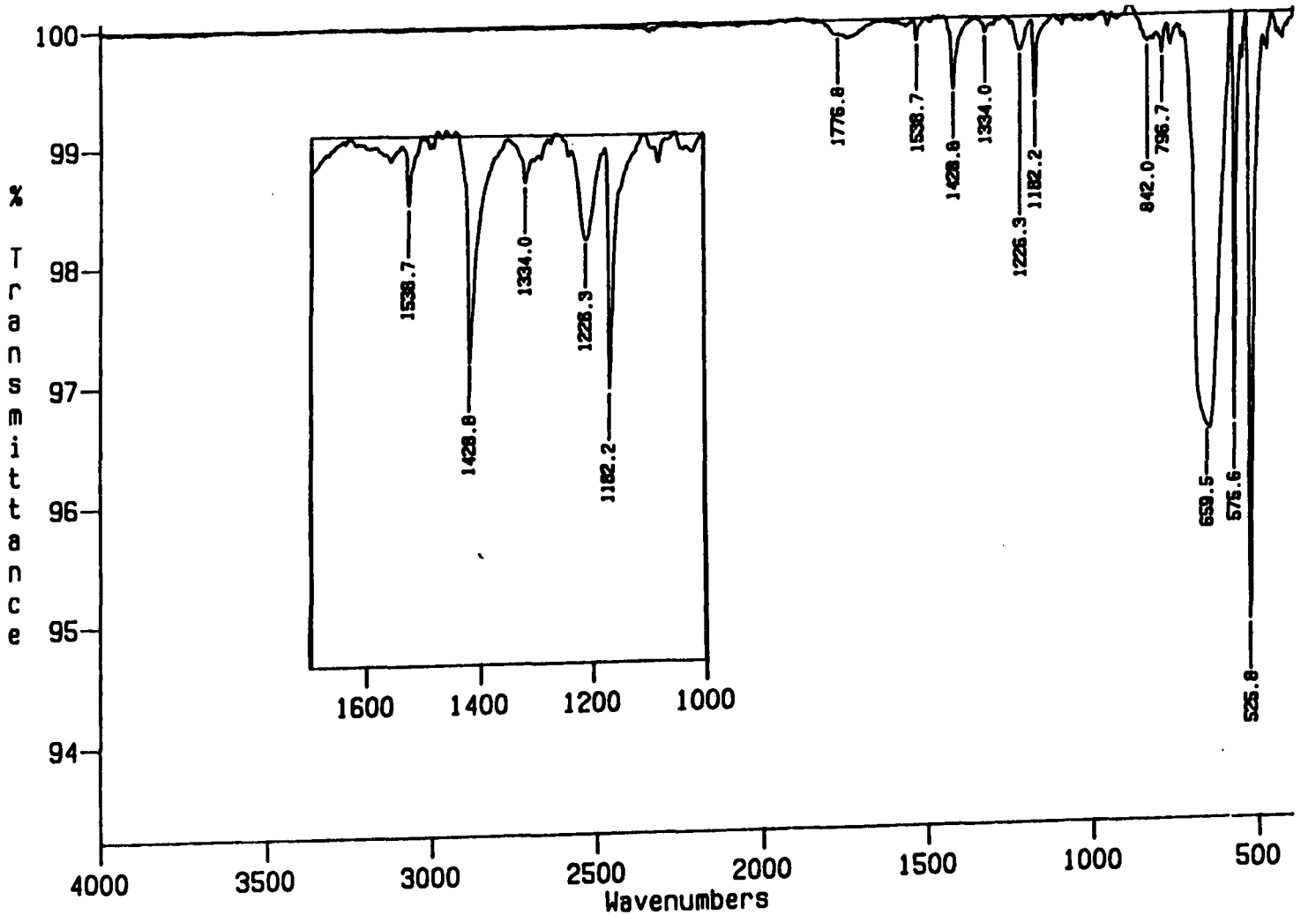

Fig. 17 Infrared spectra of C_{60} powder reacted with NO_2SbF_6 showing the broad v_3 absorption of the SbF_6^- ion at 659 cm^{-1}. The inset shows the region surrounding the $T_{1u}(3)$ and $T_{1u}(4)$ modes of C_{60}.

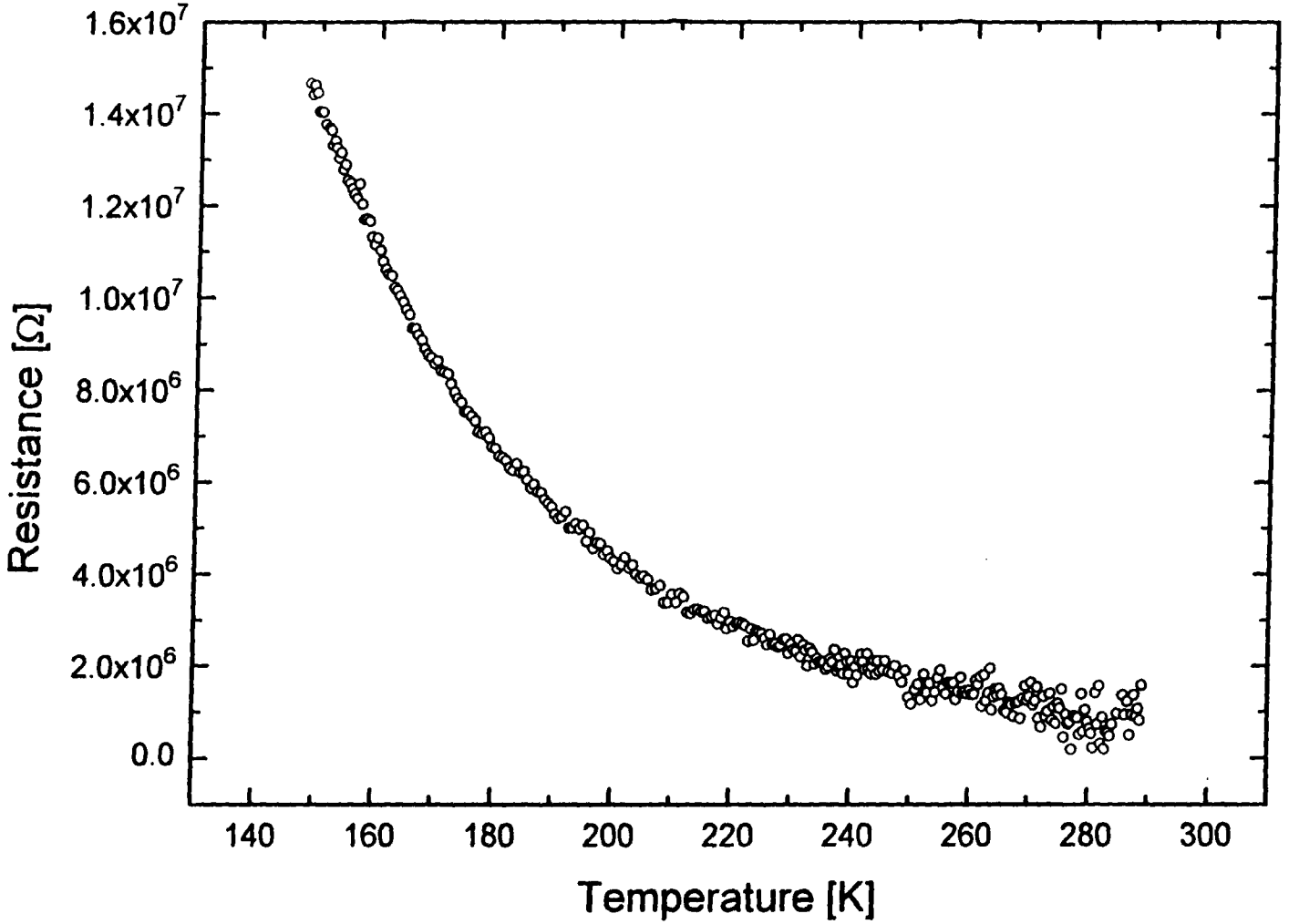

Fig. 18 The temperature dependance of the resistivity of $C_{60}(AsF_6)_{1.9}$ shows a semiconducting character, increased resistance at lower temperatures.

increased resistance at lower temperatures, is evident. With the electrical conductivity essentially thermally activated, the resistance of the sample can be expressed by the proportionality

$$R \alpha \exp (E_a/kT)$$

where R is the sample resistence, E_a is the activation energy, k is Boltzman's constant and T is the temperature. By plotting the natural log of the resistance as a function of inverse temperature the activation energy can be obtained from the equation

$$E_a = \text{slope} \times 8.62 \times 10^{-5} \text{ eV/K}.$$

A typical curve used to determine the activation energy is presented in Figure 19. A number of runs of the $C_{60}(AsF_6)_{1.9}$ samples resulted in an activation energy of 0.12 ± 0.05 eV. The resistivity of the samples was determined by

$$\rho = RA / l$$

where R is the measured resistence, A is the cross sectional area of the sample, and l is the separation between voltage contacts. The $C_{60}(AsF_6)_{1.9}$ samples were determined to have a room temperature resistivity of the order 10^5 Ω cm.

Resistivity measurements at room temperature indicated that the pressed powder sample of C_{60} reacted with NO_2PF_6 had a very high resistivity of the order 10^7 Ω cm, leading to complications in achieving data of resistance versus temperature. The C_{60} powder reacted with NO_2SbF_6 also showed very high electrical resistivity.

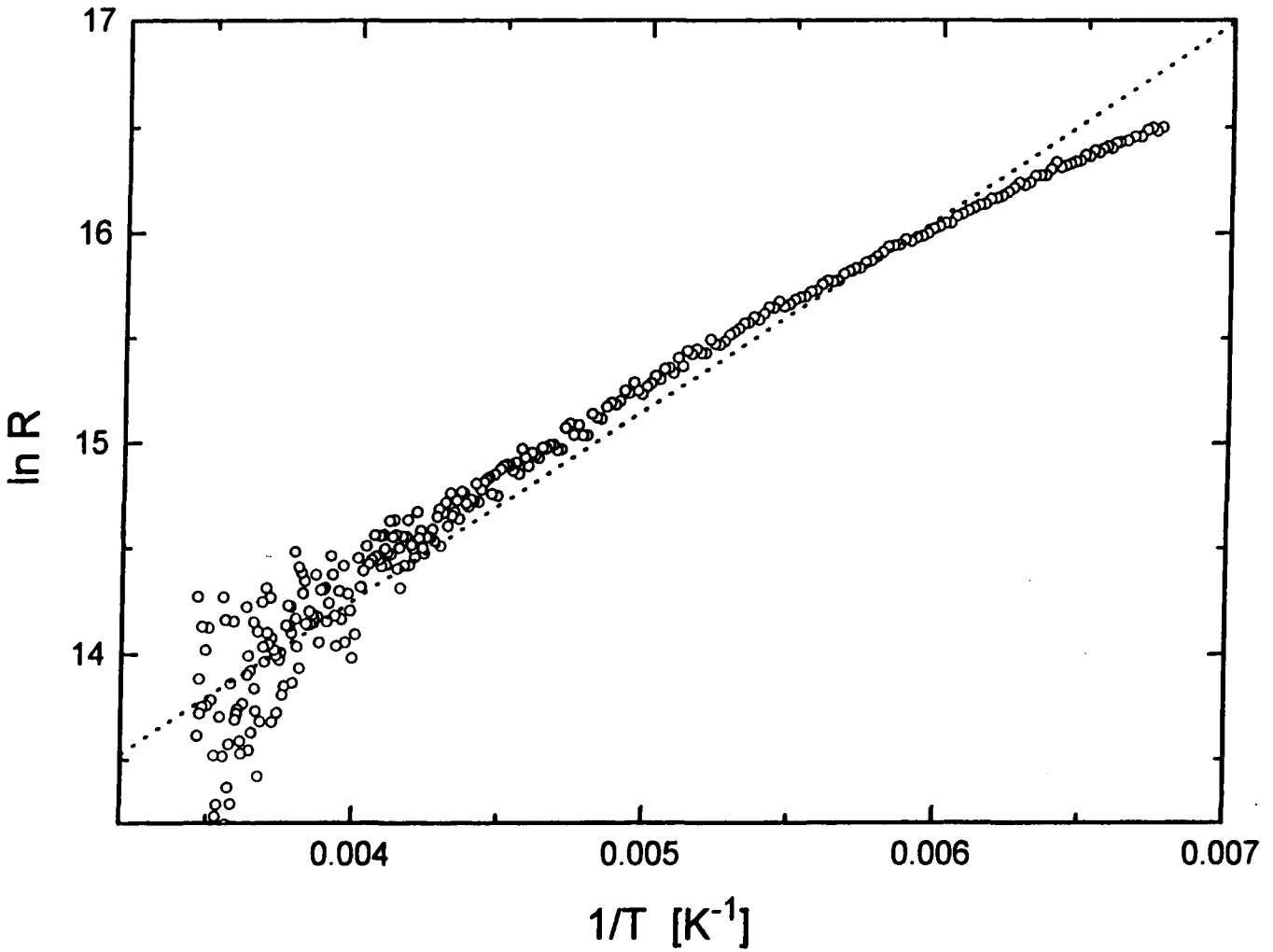

Fig. 19 A plot of the log of resistance versus inverse temperature for the $C_{60}(AsF_6)_{1.9}$ sample leads to an activation energy of 0.12 ± 0.05 eV.

Chapter 5

DISCUSSION

5.1 The $C_{60}(AsF_6)_{1.9}$ compound

The region of interest, 1700 to 400 cm^{-1}, in $C_{60}(AsF_6)_{1.9}$ is shown in Fig. 20. The absence of the very strong stretching modes at 811 cm^{-1} and 787 cm^{-1} of the trigonal-bipyramidal AsF_5 molecule, suggests that there are few, if any, of the reactant molecules trapped in the sample. The octahedral AsF_6^- molecule has six normal modes of vibration, illustrated in Figure 21. Vibrations ν_1 , ν_2 and ν_3 are Raman active, whereas only ν_3 and ν_4 are infrared active. The inset of Figure 20 shows the infrared spectrum obtained by Naulin and Bougon (1976) for the dioxygenal salt $O_2^+AsF_6^-$ showing the two absorption lines at 700 cm^{-1} and 385 cm^{-1}assigned to the ν_3 and ν_4 modes of the AsF_6^- ion (these modes were also observed by Begun *et al.* (1967) at 699 and 392 cm^{-1}). Naulin *et al.* also discuss an observed shoulder at about 680 cm^{-1} on the $\nu_3[T_u]$ IR absorption band, which was assumed to be due to a ν_3 splitting. This shoulder, on the strong broad 703 cm^{-1} absorption, also appears in the $(AsF_6)_{1.9}C_{60}$ spectrum at 681 cm^{-1}. Unfortunately, the ν_4 absorption line of the AsF_6^- ion, at 385 cm^{-1}, lies just beyond the range of the spectroscope, yet evidence of this peak may appear at the low frequency end of the spectrum. In order not to obscure evidence of this absorption by baseline fitting, the raw spectra at room temperature and during thermal decalation are presented in Figure 22. Note that the absorption at, or just below, 400 cm^{-1} decreases in size at approximately the

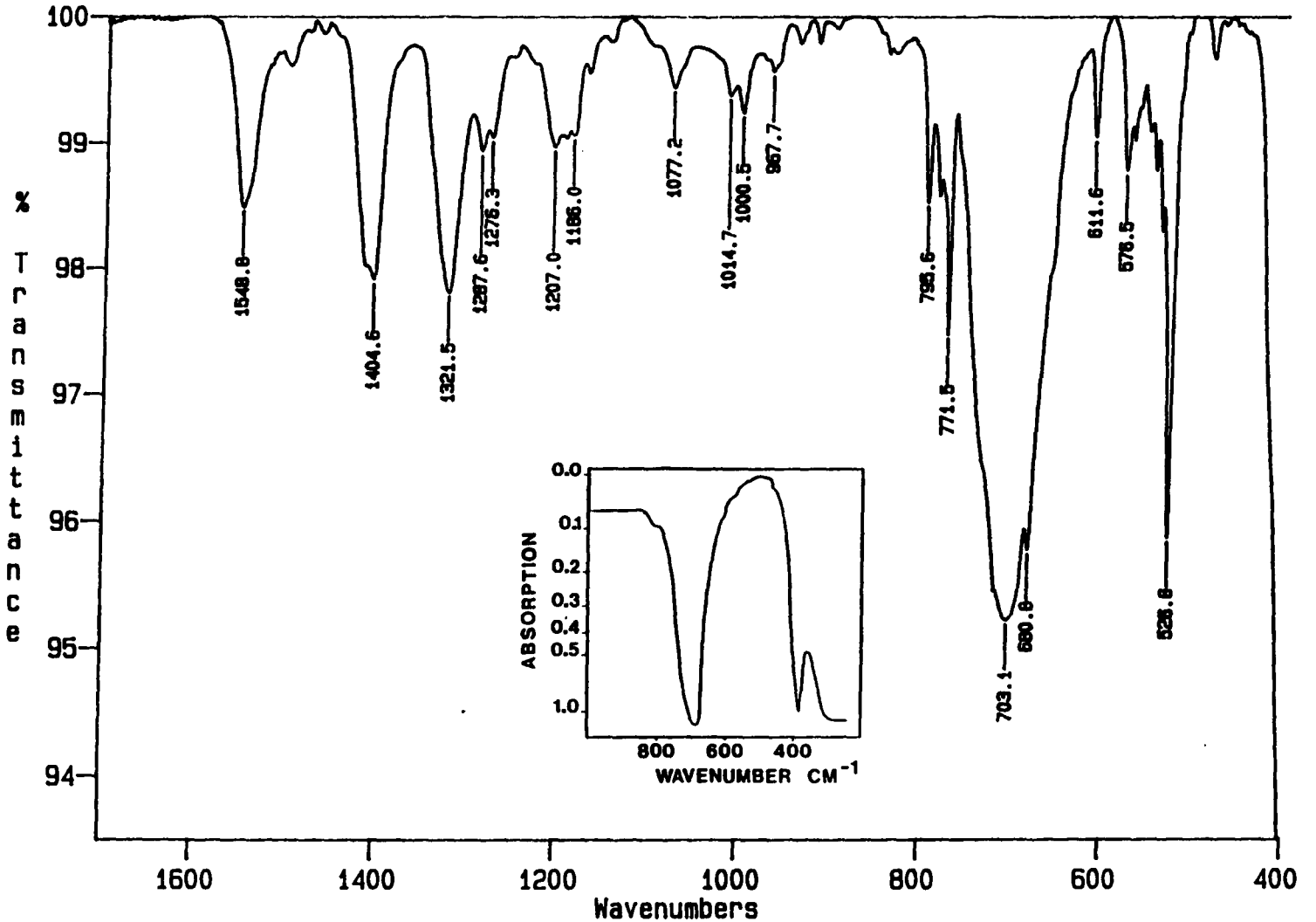

Fig. 20 IR spectra of the $C_{60}(AsF_6)_{1.9}$ compound over the range 400-1700 cm^{-1}. The inset shows the ν_3 and ν_4 absorptions of the AsF_6^- ion [Begun, 1967].

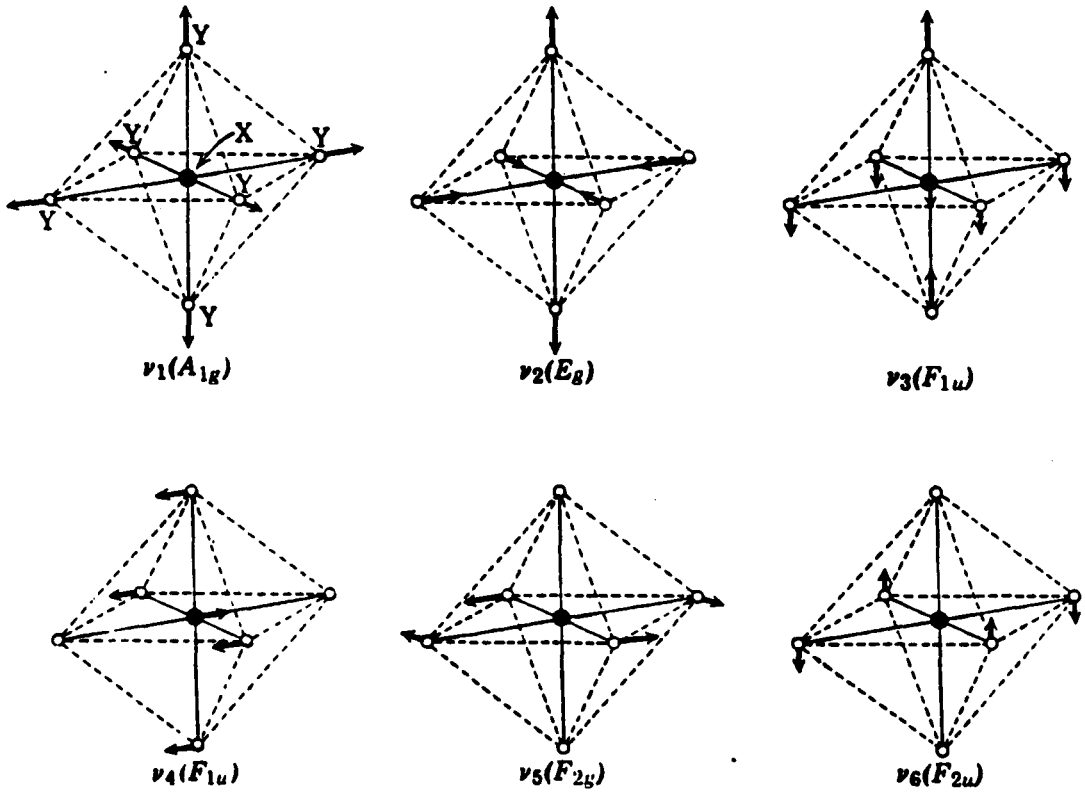

Fig. 21 The six normal modes of vibration of the octahedral XF_6^- ions (where X= P, As and Sb). The ν_3 and ν_4 vibrations are infrared active [Nakamoto, 1986].

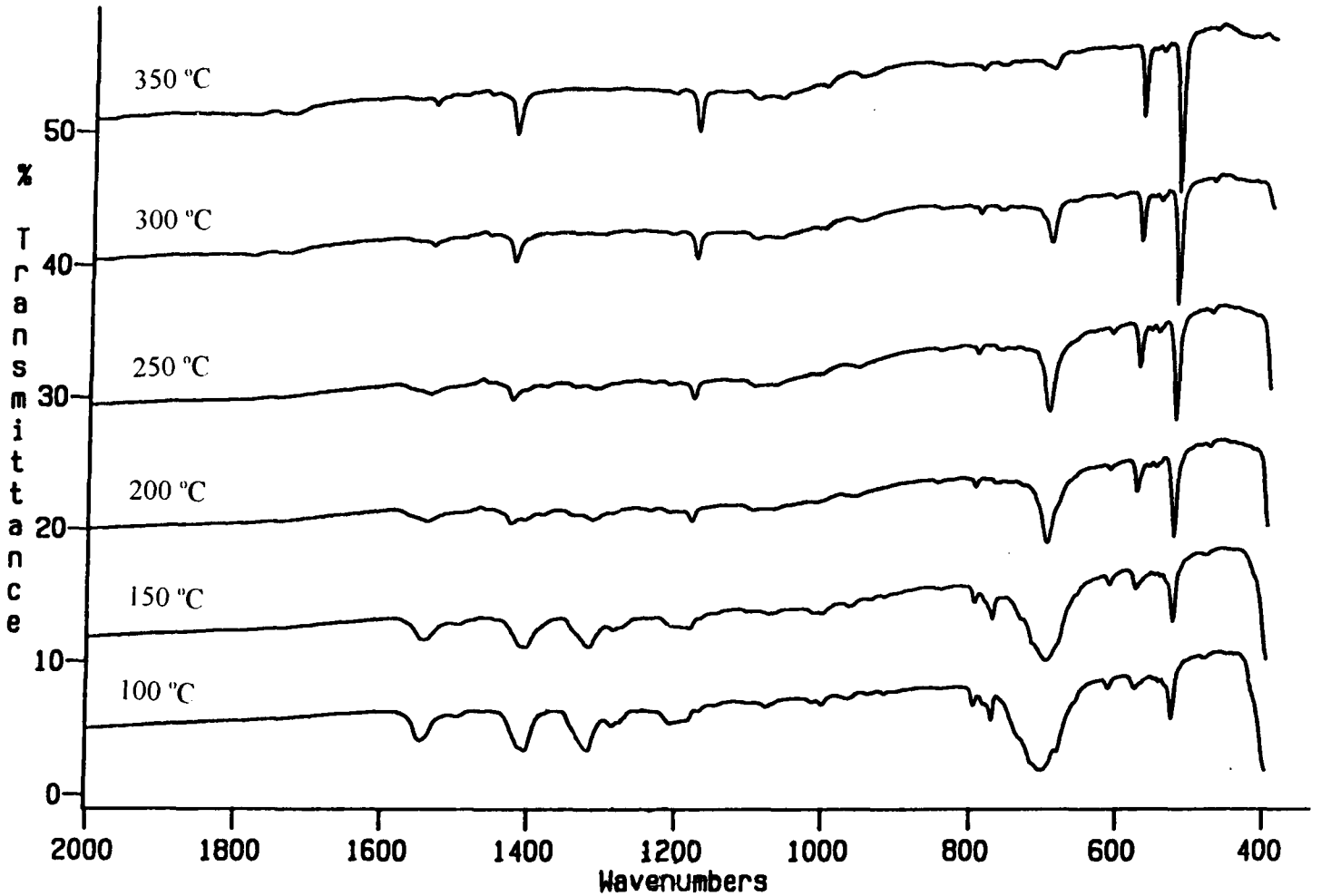

Fig. 22 Raw spectra of $C_{60}(AsF_6)_{1.9}$ during thermal decalation showing the uniform decrease of AsF_6^- lines at 703 cm^{-1} and just below 400 cm^{-1}.

same rate as the ν_3 mode at 703 cm^{-1}. Thus, the observation of the strong ν_3 absorption at 703 cm^{-1}, the 681 cm^{-1} shoulder, and the absorption near 400 cm^{-1} identifies the AsF_6^- ion in the sample.

Due to the similarities in strength and breadth of the absorptions at 1322, 1405 and 1549 cm^{-1} in $C_{60}(AsF_6)_{1.9}$, as well as their uniform changes on heating, these modes have been tentatively assigned to the splitting of the triply degenerate $T_{1u}(4)$ mode of pristine C_{60}. The possible line splitting in the $T_{1u}(4)$ mode, and the absence of splitting in the lower frequency modes, is intriguing because all the modes have the same symmetry. But a similar occurance has been observed, to a much smaller degree, even in the undoped material as it is cooled through the orientational phase transformation. Narisimham *et al.* (1992) observed the IR absorption at 1183 m^{-1} to narrow and shift slightly towards higher energy while the mode at 1429 cm^{-1} split into three lines, seperated by only a few wavenumbers, below 245K in pristine C_{60} films. These splittings were not expected *a priori* because unsplit T_{1u} modes are supported in both space groups (Fm3m and Pa3). They declared that the observed splitting pattern must therefore be related to changes in the local crystal field (ie. differences in interball coupling) which arise when the solid C_{60} goes into a rotationally locked phase.

The splitting of the $T_{1u}(4)$ mode in our samples is huge (over 100 wavenumbers) and appears much too large to be explained just by symmetry reduction of the crystal field. Indeed, a total splitting of the $T_{1u}(4)$ mode of 65 cm^{-1} was observed in Rb_1C_{60}, with no splitting of other modes, and was suggested to be due to some chemical deformation of

the C_{60} molecules, such as that arising from cycloaddition bonding [Winkler, 1995]. Regardless of the possible splitting, there is a definite shift of the $T_{1u}(4)$ line of pristine C_{60}, at 1428 cm^{-1}, to 1405 cm^{-1} in the doped $C_{60}(AsF_6)_{1.9}$ sample. Large shifts in the positions of the lines have also been observed in other doped compounds, including an observed shift of 88 cm^{-1} in the $T_{1u}(4)$ mode of a K_6C_{60} film [Pichler, 1994], which was suggested to be due to a charged phonon effect.

The $T_{1u}(3)$ mode of C_{60} is observed in the $C_{60}(AsF_6)_{1.9}$ compound crowded by higher frequency counterparts. The triplet at 1206, 1194 and 1183, all of approximately the same strength, may represent splitting of the triply degenerate mode. The pristine C_{60} mode, at 1183 cm^{-1}, becomes more dominant as the sample is thermally decalated (shown in Fig. 23, up to 200°C).

A second possible explanation is that the $T_{1u}(3)$ line shifts to higher frequencies due to intercalation, yet the three closely spaced absorptions may be contributions from more than one phase in the infrared spectrum, which are present due to non-uniform intercalation. In this case the observation of the three closely spaced absorptions, which shift in strength towards the lowest frequency with thermal decalation, may indicate a correspondence to three distinct phases in the sample (presumably $C_{60}(AsF_6)_x$ with x=2,1,0). This second hypothesis is less likely considering that the 1428cm^{-1} line in pristine C_{60} (x=0 phase) is not observed in the $C_{60}(AsF_6)_{1.9}$ spectra.

Thermal decalation of the $C_{60}(AsF_6)_{1.9}$ powder was achieved by heating the sample in a vacuum, with temperatures ranging up to 350°C. The infrared spectra, taken at

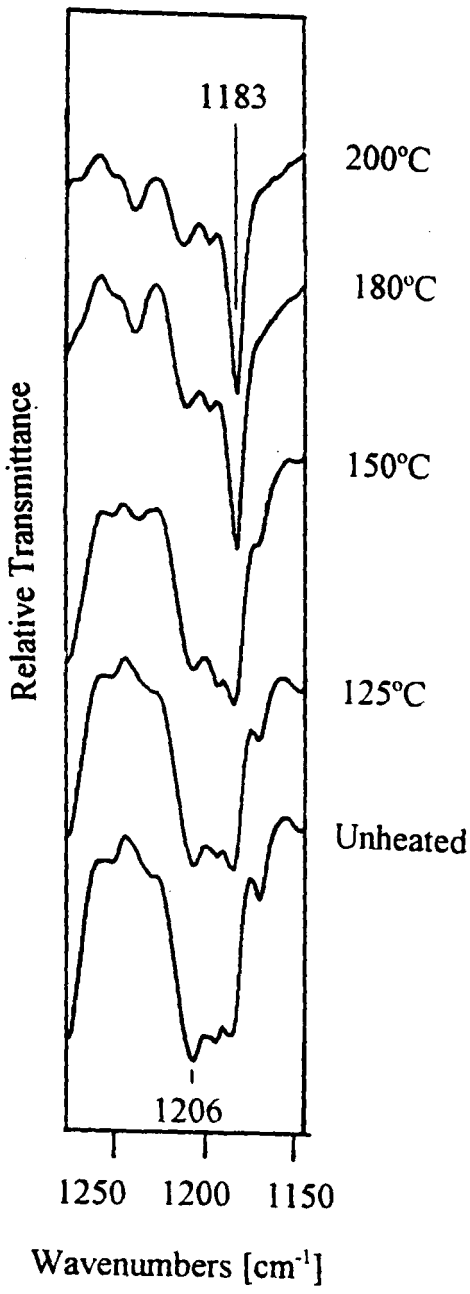

Fig. 23 The 1183 cm^{-1} line of pristine C_{60} is accompanied by closely spaced counterparts at 1206 and 1194 cm^{-1} in the unheated sample.

certain temperature intervals (after cooling again to room temperature), showed little change at temperatures below 150°C. Further heating of the powder resulted in a decrease of the AsF_6^- absorption features at 703 and 681 cm^{-1} as well as the proposed ν_4 absorption just below 400 cm^{-1}. The three strong broad absorption lines at 1549, 1406 and 1322 cm^{-1} decreased in intensity as the 1428 cm^{-1} line of pristine C_{60} emerged with further heating. As well, the higher frequency counterparts to the $T_{1u}(3)$ line at 1183 cm^{-1} decreased in intensity. Throughout the heating process the low frequency $T_{1u}(1)$ and $T_{1u}(2)$ modes of C_{60}, at 527 and 576 cm^{-1}, remained unshifted in frequency. Following heat treatments at 350°C there was little trace of the AsF_6^- ion. The return of the strong pristine C_{60} lines in the IR spectra, at 527, 576, 1183 and 1428 cm^{-1}, indicated the successful decalation of the sample, with the buckyball retaining its molecular identity. As well, x-ray diffraction data shows that the crystal structure of $C_{60}(AsF_6)_{1.9}$, which had expanded to bct to accomodate the AsF_6^- ion, changed to the fcc structure of the C_{60} starting material. The thermal decalation of the $C_{60}(AsF_6)_{1.9}$ is assuredly accompanied by the production of gases, such as AsF_3 and AsF_5. Although collection and analysis of these decalation biproducts was discussed, technical difficulties have not yet made it possible.

5.2 C_{60} powder reacted with NO_2PF_6

The infrared spectrum of the C_{60} powder reacted with NO_2PF_6 in liquid SO_2 shows a number of features in the low frequency portion of the spectra. The PF_6^- ion is identified in the sample by the broad ν_3 absorption, reported by Begun and Rutenberg (1967) at 830

cm^{-1} , as well as by the sharp ν_4 mode reported at 558 cm^{-1}. Also, it should be noted that neither the strong absorption at 2360 cm^{-1} nor the weaker absorption at 570 cm^{-1} [Nebgen, 1965] of NO_2^+ are observed, indicating that the powder is not a simple mixture of NO_2PF_6 and C_{60}. Lines in the IR spectrum appear at 526, 576, 1182 and 1429 cm^{-1}, unshifted from those of C_{60}, but the $T_{1u}(4)$ line is flanked by two neighbouring absorptions, at 1538 and 1334 cm^{-1}, that are close in frequency to the observed lines at 1549 and 1322cm^{-1} in $(AsF_6)_{1.9}C_{60}$. Although the $T_{1u}(4)$ mode remains at 1429 cm^{-1}, it appears assymetrically broadened on the lower frequency side, which may correspond with the observed downshift of this line in the arsenic hexafluoride sample. These features are similar to those observed with the intercalation of the AsF_6^- ion, but are not nearly as pronounced. The NO_2 gas observed during the reaction process indicated that the NO_2^+ ions, dissociated in the liquid SO_2 , had oxidized the C_{60} molecules. The presence of the PF_6^- ion was identified in the sample by infrared data. But this two step method of intercalating ions to produce a charge neutral material may need longer reaction times to produce homogenous samples, for the X-ray diffraction pattern showed only small changes from that of pure C_{60}. Heat treatment of the PF_6^- compound at 350°C under vacuum yielded an IR spectrum with strong absorptions at 526, 576, 1182 and 1429 cm^{-1}. These values, close to those of pristine C_{60}, combined with the disappearance of lines attributed to PF_6^-, indicated the decalation of the sample, with no disruption of the buckyball.

5.3 C_{60} powder reacted with NO_2SbF_6

The reaction with NO_2SbF_6 and C_{60} shows no absorption due to the NO_2^+ ion at 2360 cm^{-1} or 570 cm^{-1} [Nebgen, 1965] in the infrared spectrum. It does, however, show the strong broad absorption of SbF_6^- at 660 cm^{-1} which is very close (for such a broad peak) to the reported value of 669 cm^{-1} [Begun, 1967]. The ν_4 mode of SbF_6^-, at 350 cm^{-1} lies below the range of the spectrometer. Again, the observed lines of the hexafluoride anion, without the NO_2^+ ion indicates that the resulting powder is not simply a mixture of C_{60} and NO_2SbF_6. Although the C_{60} peaks are unshifted, the $T_{1u}(3)$ line, at 1182, has a higher frequency counterpart at 1226, and the $T_{1u}(4)$ line is flanked by absorptions at 1538 and 1334cm^{-1}. These features, although small, may correspond to the splitting observed in the high frequency modes of $(AsF_6)_{1.9}C_{60}$. Heat treatment of the powder at 350°C, led to an IR spectra almost identical to pristine C_{60} indicating the decalation of the sample, with no disturbance of the molecule.

5.4 Additional features

There is no evidence in the IR spectra to suggest the presence of SO_2 solvent in the samples, which has absorptions at 1147, 517 and 1351 cm^{-1} [Maillard, 1975]. As well, the 739 cm^{-1} [Clark, 1974] absorption line of the stable AsF_3 molecule is not observed in the $C_{60}(AsF_6)_{1.9}$ sample. The AsF_3 molecule also has absorptions at 262, 337 (below the range of the spectrometer) and 699 cm^{-1} (corresponding to an observed line attributed to AsF_6^-).

There are a number of other absorption lines, primarily in the $C_{60}(AsF_6)_{1.9}$ spectrum, which are unaccounted for. Extreme care was taken to remove any traces of moisture from the reaction vessels, considering arsenic pentafluoride in the presence of moisture generates HF. HF has a single IR absorption at 4139 cm^{-1} [Herzberg, 1950], too high to be observed. However, HF quickly converts glass to SiF_4 and the AsF_5 to $AsOF_3$. But niether the SiF_4 absorption at 1030 cm^{-1} [Clark, 1971] nor the strong $AsOF_3$ peaks at 811 and 784 cm^{-1} [Mitra, 1958] are observed.

Differences in the lattice dynamics between the fullerides and the fullerite may arise from a number of factors. The introduction of ions into the interstitial sites changes the crystal structure and symmetry and may give rise to new optic modes. New phonon modes are discussed by M. Dresselhaus *et al.* (1992) for doped C_{60} in the spacegroups T_h^6 (fcc) and T_h^5 (bcc). However, the body centered tetragonal phase, clearly observed in the $(AsF_6)_{1.9}C_{60}$ compound, is a lower symmetry space group (where the C_{60} molecules would occupy sites with C_{2v} symmetry), and is only briefly mentioned in the paper.

Another important factor is the charge transfer from the molecule to the acceptor ions, which will alter the bond bending and bond stretching force constants. This may explain why the higher frequency $T_{1u}(3)$ and $T_{1u}(4)$ infrared modes of C_{60} are affected by the intercalation of the ions, while the lower ones are not. The tangential motion of the carbon atoms, in the higher frequncy modes, stretch and bend the bonds to a greater degree than the progressivly more radial motion of the lower frequency modes.

Additional features in many of the alkali metal fullerides have been assigned to IR forbidden and second order modes which have become IR active due to charge transfer (which can dress many of the modes with a dipole moment). Martin *et al.* (1993) illustrated how the addition (or reduction) of electrons to a complex molecule can enhance the strength of a "silent" IR active phonon. Figure 24(a) depicts an eigenmode of the molecule, characterized by two pairs of atoms oscillating in opposite phase. This mode is "IR active" in the sense that it has odd symmetry. However, as long as only symmetric electronic states are allowed, the mode is "silent" since there is no net dipole moment in the direction of the electric field. In Figure 24(b) asymmetric states are allowed (ie. electron transfer between the two pairs of atoms). The electron transfer naturally couples to the atomic displacements via the rearrangement of electronic states, and it also generates an electric dipole moment. Rice and Choi (1992) formulated a model in which coupling can even dress *gerade* (symmetric) modes with a dipole moment, a behaviour which is well known for organic charge transfer systems. This model was used to describe the IR spectra of the K_3C_{60} compound, in which observed features were assigned to the *gerade* modes of A_g and H_g symmetry [Pichler, 1993]. The majority of the fundamental modes are not opticly active in pristine C_{60} and consequently cannot be directly observed. The calculations of the mode frequencies are not extremely accurate, but are presented for reference in Table II of chapter 2. Combining this with the possible shift of eigenfrequencies due to intercalation, makes the work of assigning features in the IR spectra to forbidden modes extremely difficult. Although some assignments of absorption

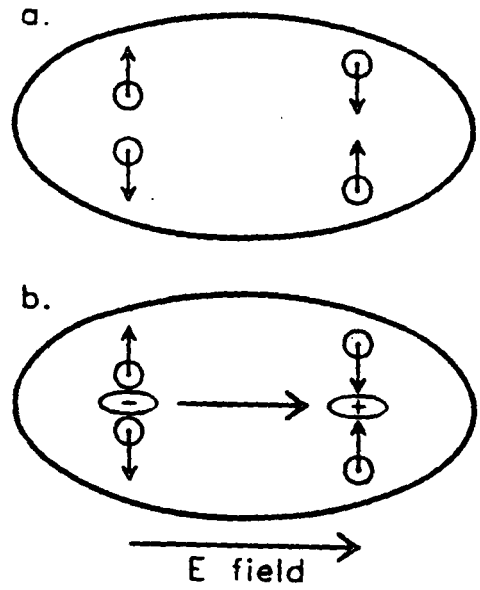

Fig. 24 Schematic illustration of charge transfer induced infrared activity. The arrowed circles represent atoms moving within a single "molecule"; the symmetry of the oscillation is odd. In (a) only even electronic states are allowed and therefore the strength of the IR-active vibration is small. In (b) the electron transfer couples the mode to the external field by introducing a dipole moment [Martin, 1993].

features in $(AsF_6)_{1.9}C_{60}$ can be speculated (such as the sharp line at 772 cm^{-1} lying very close to the $H_g(4)$ mode observed at 774 cm^{-1} in the Raman spectra), a more detailed analysis is not only in principle very complicated but also inappropriate, as shifts of Raman active modes, and theotical shifts of optically inactive modes, have not been studied for acceptor intercalated C_{60} materials.

5.5 Interstitial sites

X-ray powder diffraction of $C_{60}(AsF_6)_{1.9}$ has indicated that the C_{60} lattice shifts to a bct structure with a=12.794Å and c=12.426Å. Schematic structures of the expanded C_{60} lattice are shown in Figure 25 with the buckyballs depicted as spheres of radius 3.55Å. The location of possible interstitial sites are shown occupied by smaller spheres of radius 2Å. The upper two figures, (a) and (b), represent crystal structures with tetrahedral site occupancy, while the lower figure, (c) and (d), present the possible octahedral sites. The sizes of the possible interstitial sites for bct packing of rigid spheres of radius 3.55Å are calculated in Appendix A and summarized in Table IV.

The octahedral AsF_6^- ion has bond lengths of 1.69Å. Combining this with the ionic radius of fluorine, 1.33Å, enables the ion to be represented by a sphere of radius ~3Å [Brown, 1996]. The best structural fit for the AsF_6^- ions is obviously the large tetrahedral sites depicted in Figure 25 (a), which, when filled, also corresponds closely with the observed stoichiometry of the material. Yet the orientation of the octahedral AsF_6^- ion is unknown, and it may be oriented to fit into other possible sites as well.

Fig. 25 Interstitial sites in the bct lattice of $C_{60}(AsF_6)_{1.9}$. Figures (a) and (b) represent crystal structures with tetrahedral site occupancy, and figures (c) and (d) show filled octahedral sites.

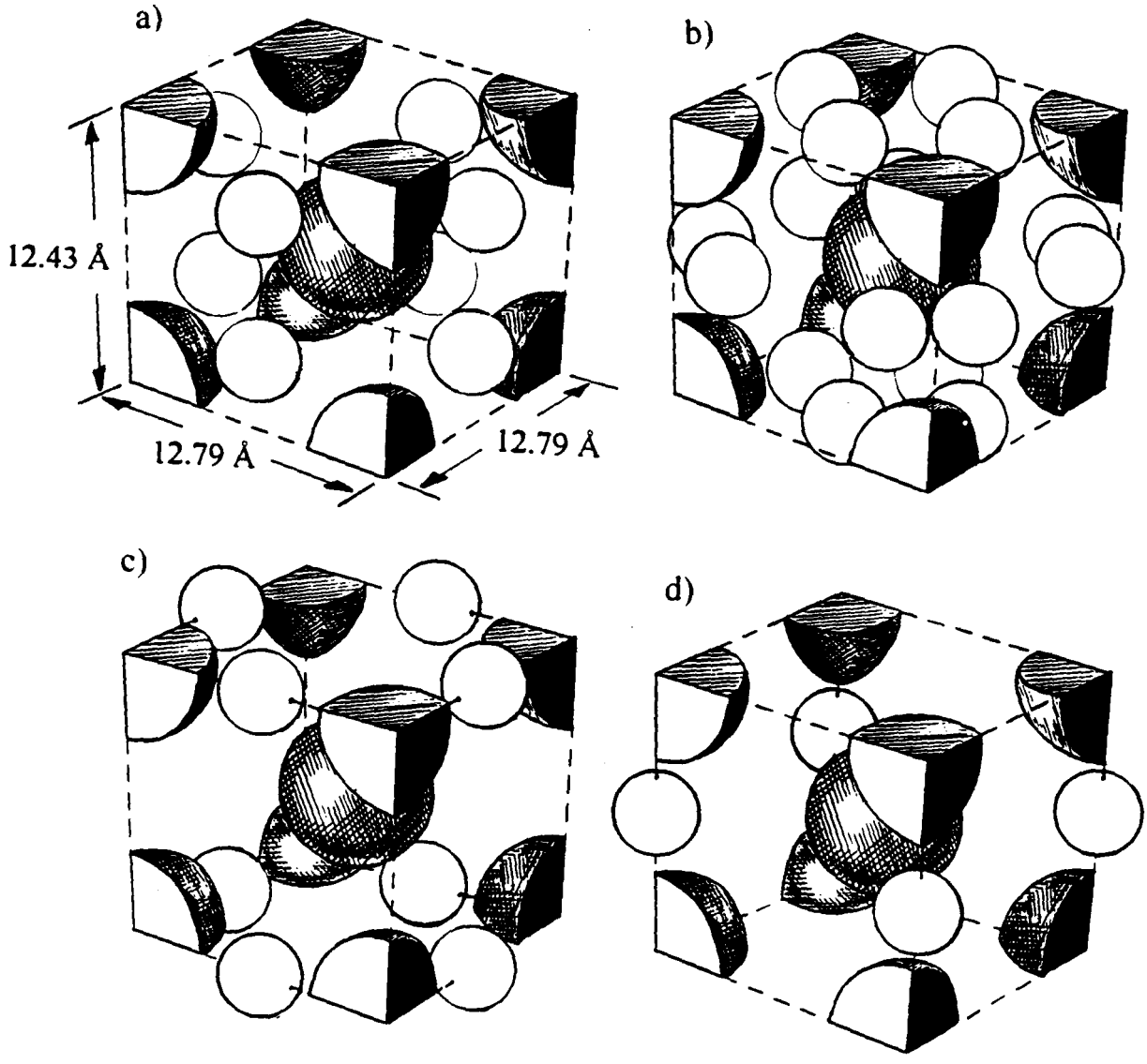

Table IV. Interstitial sites in bct C_{60} with a=12.794Å and c=12.426Å, showing the number of sites per C_{60} molecule, the coordination number and radius.

Type	No. per C_{60}	Coordination Number	Radius (Å)
a)	2	4	3.1
b)	4	4	2.7
c)	1	6	2.9
d)	0.5	6	2.7

5.6 Resistivity measurements of $C_{60}(AsF_6)_{1.9}$

Upon cooling, the $C_{60}(AsF_6)_{1.9}$ sample exhibited an exponential resistance increase with decreasing temperature typical of a semiconductor with an activation energy of 0.12 $\pm$ 0.05 eV, and a room temperature resistivity on the order of 10^5 Ω cm. However, as the temperature decreased the resistance increased at a slightly greater rate than expected for pure semiconducting behaviour indicating that some charge may be mobile by processes other than thermal excitation of carriers.

Of particular note, in the resistivity measurements, is the lack of a transition around 250K. A disturbance would be expected for any undoped sample due to the sudden change of the lattice parameter during the orientational ordering phase transition. Discontinuities in the resistance as a function of temperature have been observed near

250K in other intercalated C_{60} compounds, but usually for samples with larger grain sizes such as films or crystals [Winkler, 1995]. The lack of such a disturbance in the $C_{60}(AsF_6)_{1.9}$ suggests a relatively homogenous sample with few regions of pristine C_{60}.

Chapter 6

CONCLUSIONS

Study of the infrared spectra of the $C_{60}(AsF_6)_{1.9}$ compound during thermal decalation, combined with x-ray diffraction and resistivity measurements has confirmed the existence of this C_{60} compound intercalated with acceptor molecules. Infrared spectroscopy also yielded strong evidence for the interaction of C_{60} with other group V hexafluoride ions, PF_6^- , and SbF_6^-.

The broad ν_3 absorption at 703 cm^{-1} , as well as a shoulder at 680 cm^{-1} , and evidence of the sharp ν_4 absorption just below 400 cm^{-1} identifies the octahedral AsF_6^- ion in the sample of C_{60} reacted with AsF_5. Evidence of AsF_5 ,such as the very strong stretching modes at 811 cm^{-1} and 787 cm^{-1} of the trigonal-bipyramidal molecule, was unobserved. The low frequency $T_{1u}(1)$ and $T_{1u}(2)$ modes of C_{60}, at 527 and 576 cm^{-1}, in the IR spectra of the samples appear unaffected by intercalation. The $T_{1u}(4)$ mode of the $(AsF_6)_{1.9}C_{60}$ exhibits a downshift in frequency from the 1428 cm^{-1} absorption line of pristine C_{60} to 1406 cm^{-1}. As well, this triply degenerate mode exhibits splitting leading to neighbouring peaks at 1549 and 1322 cm^{-1}. Three closely spaced peaks at 1206, 1194 and 1183 have been tentatively assigned to splitting of the $T_{1u}(3)$ mode.

The diffusion of the large molecular dopants within crystallites of solid C_{60} was facilitated by using a solid-solution method of AsF_5 gas, dissolved in SO_2, reacted with C_{60} powder. The success of this method was noted by the absence of the absorption at 1428

cm^{-1} of pristine C_{60} in the $C_{60}(AsF_6)_{1.9}$ infrared spectra, and the lack of a disturbance at ~250K in the resistivity measurements indicating that there are few regions of undoped material in the sample.

Thermal decalation of the $C_{60}(AsF_6)_{1.9}$ sample was performed in vacuum, with temperatures ranging up to 350°C. After cooling again to room temperature, infrared spectra of the powder were taken. Little change in the IR spectra was observed at temperatures below 150°C. As the powder was heated further, the AsF_6^- features, at 703 and 681 cm^{-1} decreased in intensity. As well, the proposed ν_4 absorption, just below 400 cm^{-1}, also decreased at a similar rate. Following heat treatments at 350°C there was little trace of the ion in the IR spectra. In addition, the three strong broad absorption lines at 1549, 1406 and 1322 cm^{-1} decreased in intensity, as the 1428 cm^{-1} line of pristine C_{60} emerged. The lines surrounding the $T_{1u}(3)$ mode, at 1206 and 1194 cm^{-1} also diminished, as the 1183 cm^{-1} line increased in relative intensity. The emergence of the strong C_{60} lines in the infrared spectra, at 527, 576, 1183 and 1429 cm^{-1} with few other features, indicated that the buckyball had retained its molecular identity throughout the intercalation and decalation process. X-ray diffraction data also indicated that the fcc lattice of C_{60}, which had reoriented to a bct structure for the intercalation of the AsF_6^- ion, shifted back to the C_{60} structure after heat treatments, indicating the successful decalation.

In the sample of C_{60} reacted with NO_2PF_6, both the broad ν_3 absorption of the octahedral PF_6^- ion at 830 cm^{-1} and the sharp ν_4 at 558 cm^{-1} were observed. However, the broad absorption of NO_2^- was not observed, indicating that the sample was not a simple

mixture of the two powders. Evidence of the NO_2^- ion oxidizing the C_{60} to become NO_2 gas was observed during the reaction process, as the colourless SO_2 liquid became brown in colour. The C_{60} powder reacted with NO_2PF_6 also had small absorptions at 1539 and 1334 cm^{-1} flanking the $T_{1u}(4)$ mode, which also showed broadening on the low frequency side. These features may correspond to the similar, but much enhanced, features seen in the $C_{60}(AsF_6)_{1.9}$ compound. Heat treatment of the powder at 350°C led to an IR spectrum very similar to that of pure C_{60}.

The presence of the SbF_6^- ion, in its respective sample, was identified by the strong ν_3 absorption at 660 cm^{-1}, while the ν_4 mode lay below the range of the spectrometer. Again, the presence of the NO_2^- ion was unobserved in the IR spectra, while evidence of brown NO_2 gas, dissolved in SO_2, was observed during the reaction process. Absorptions at 1539 and 1334 cm^{-1}, flanking the $T_{1u}(4)$ mode, were also observed in the IR spectra. Thermal decalation of the sample, identified by the return of only the four strong C_{60} lines in the IR spectra, was achieved by heating to 350°C in vacuum. For these large ions, and using NO_2 as an oxidizer, diffusion is not facile and reactions may need to be carried out for extended periods of time in order to produce bulk samples.

Additional features in the IR spectra, which occur in the greatest abundance in the highly doped $C_{60}(AsF_6)_{1.9}$ compound, remain unassigned. The introduction of ions into the interstitial sites changes the crystal structure and symmetry and may give rise to new optic modes. The charge transfer also introduces ionic forces and the possibility of changes in

the intermolecular optic modes. Thus, interpreting all of the differences between the vibrational spectra of fullerite and the fullerides is not a straightforward matter.

Appendix A

Geometrical determination of the radius of interstitial sites in $(AsF_6)_{1.9}C_{60}$

Powder x-ray diffraction patterns determined the structure of the $(AsF_6)_{1.9}C_{60}$ sample to be body centered tetragonal (bct) with cell dimensions a=12.794Å and c=12.426Å. Using rigid spheres of radius 3.55Å for the C_{60} molecules [Fischer, 1991], the crystal structure is represented in Fig. A1 a) and b) for tetrahedral site occupancy and Fig. A1 c) and d) for octahedral site occupancy. The rigid spheres shown occupying these sites have a radius of two angstroms.

Due to the shortened c axis, with respect to the a and b axes, all tetrahedral sites are not identical. Consider first the tetrahedral sites depicted in Fig A1 a), and specifically the occupied interstitial site labeled A. With the origin labeled as O, this site has four nearest neighbour C_{60} molecules centered at (x,y,z) = (0,0,0), (a,0,0), (a/2,a/2,c/2) and (a/2,-a/2,c/2). Due to symmetry considerations the interstitial site A is located at (a/2, 0, z), where z is a variable denoting the vertical distance from the xy plane. The size of this interstitial site is limited by the distance from the center of the site to the neighbouring C_{60} surfaces. The distances from the centers of neighbouring buckyballs to the site center is denoted in Fig. A2 by the vectors $\mathbf{r}_1$ and $\mathbf{r}_2$ which have the following magnitudes;

$$|\mathbf{r}_1| = \sqrt{(a/2)^2 + z^2} \qquad \text{(A1)}$$

and

$$|\mathbf{r}_2| = \sqrt{(a/2)^2 + (c/2 - z)^2} \qquad \text{(A2)}$$

Fig. A1 Interstitial sites of the bct lattice of $C_{60}(AsF_6)_{1.9}$. Due to the shortened c axis, with respect to the a and b axes, there are two types of tetrahedral and two types of octahedral interstitial sites.

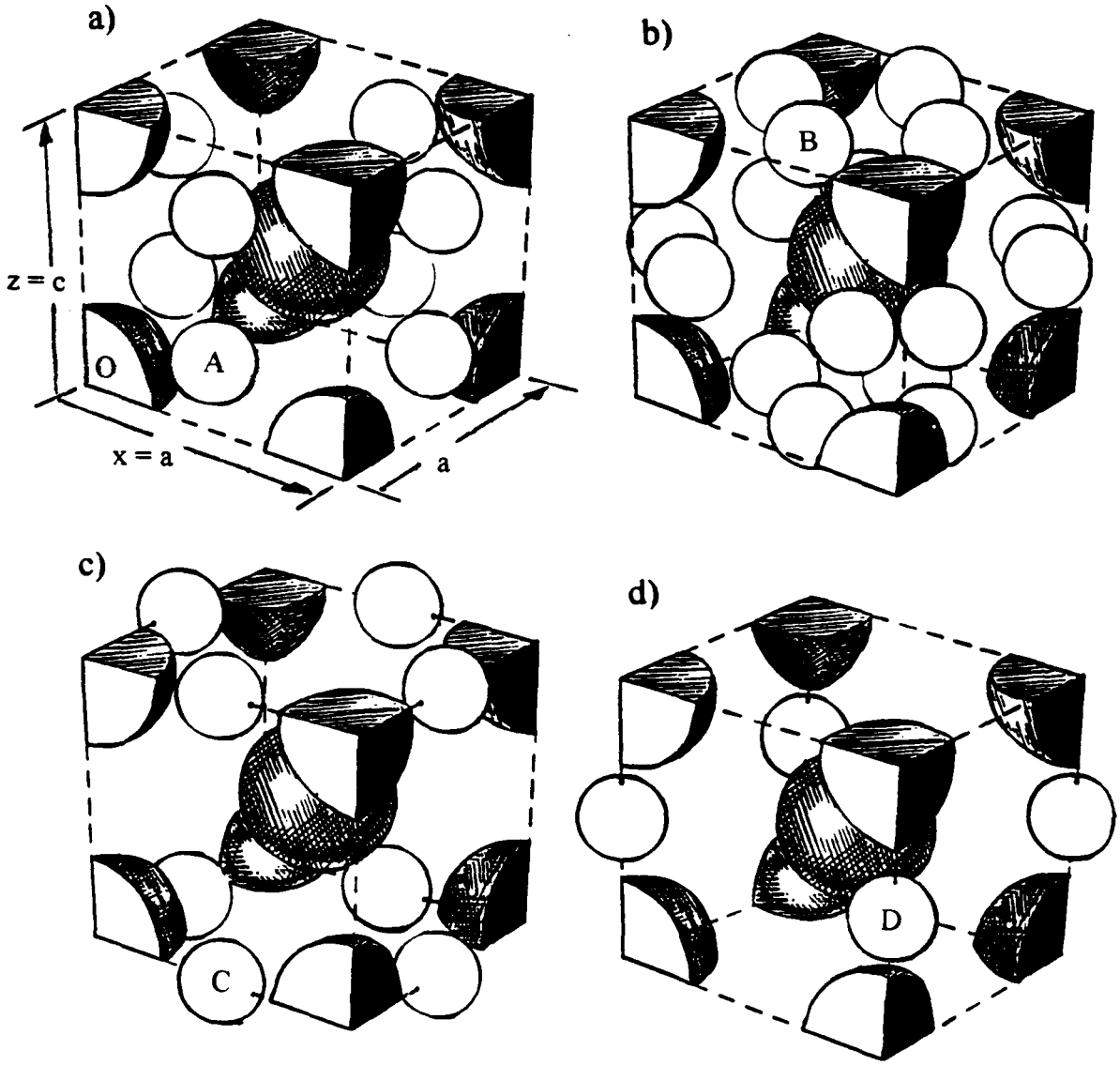

Fig. A2 Distances from the centers of neighbouring buckyballs to the center of interstitial site A are given by the magnitudes of vectors $\mathbf{r}_1$ and $\mathbf{r}_2$.

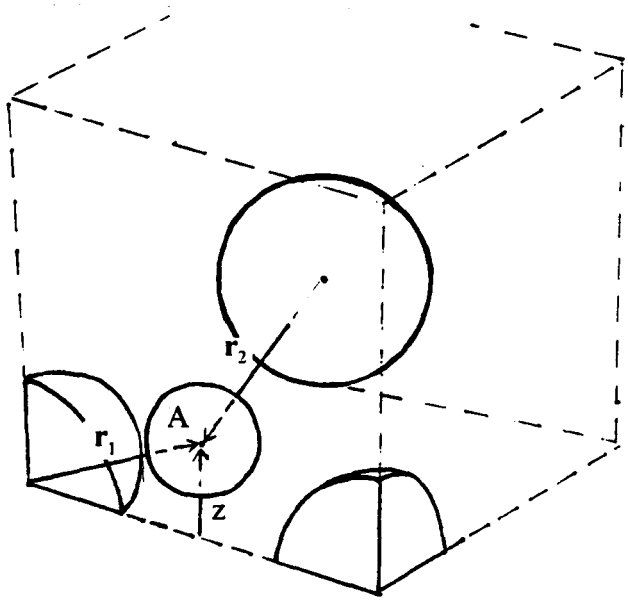

Fig. A4 The size of the interstitial site B is limited by other filled sites of the same type, shown here on the xy plane.

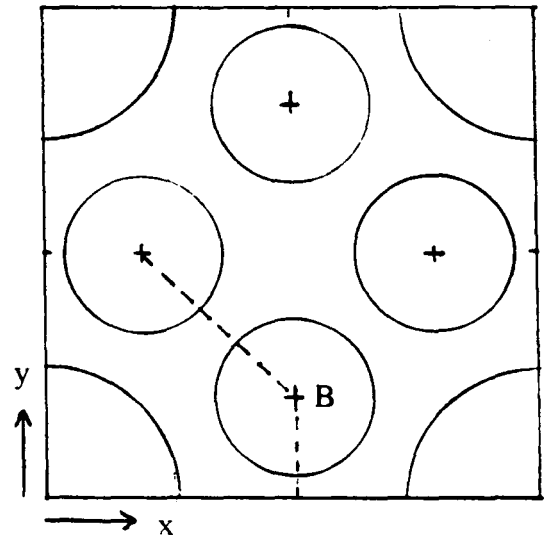

Subtracting the C_{60} radius from these lengths gives constraints for the maximum size of the interstitial radius,

$$r_A \leq \sqrt{(a/2)^2 + z^2} - r_{C60} \quad \text{(A3)}$$

$$r_A \leq \sqrt{(a/2)^2 + (c/2 - z)^2} - r_{C60} \quad \text{(A4)}$$

If the neighbouring interstitial site at (a/2, 0, c-z) is also filled then two more constraints are added so that the site spaces don't overlap,

$$r_A \leq z \quad \text{(A5)}$$

$$r_A \leq c/2 - z \quad \text{(A6)}$$

These constraints, equations A3 to A6, are plotted in Fig. A3. The largest interstitial radius for this site occurs at $z = r_A = 3.11$Å.

The remaining tetrahedral sites, shown in Fig. A1 b), have similar constraints with respect to neighbouring C_{60} molecules. For the interstitial site, labeled B, at (a/2, y, c) the constraints are,

$$r_B \leq \sqrt{(a/2)^2 + y^2} - r_{C60} \quad \text{(A7)}$$

$$r_B \leq \sqrt{(c/2)^2 + (a/2 - y)^2} - r_{C60} \quad \text{(A8)}$$

With all sites of type (b) filled, two more constraints become apparent:

$$r_B \leq y \quad \text{(A9)}$$

$$r_B \leq (a/2) - y \quad \text{(A10)}$$

As well, a fifth constraint limits the interstitial radius due to intercalant molecules located diagonally across the xy plane (shown in figure A4),

$$r_B \leq \sqrt{(a/2 - y)^2 + (a/2 - y)^2}/2 \quad \text{(A11)}$$

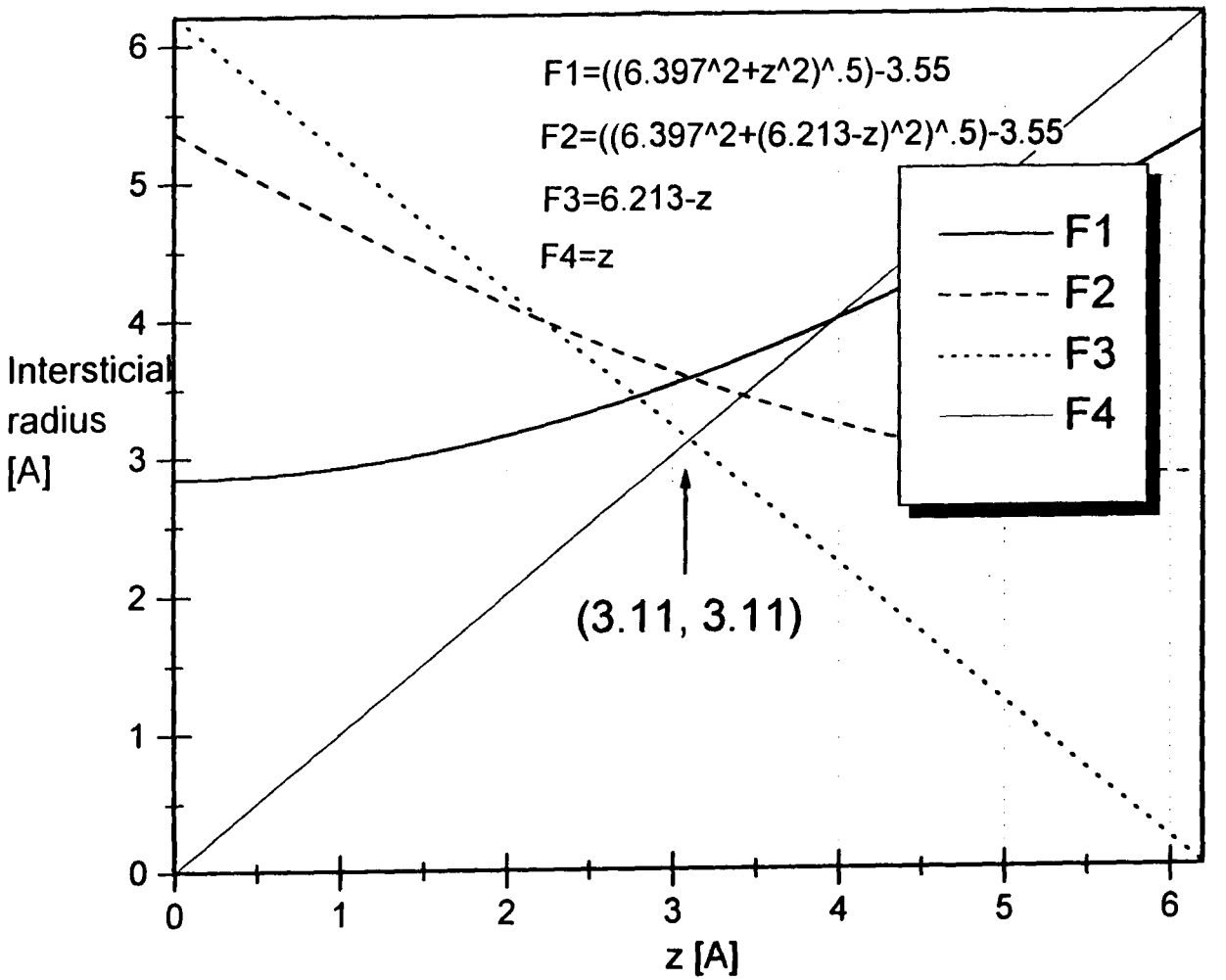

Fig. A3 Constraints on the radius of tetrahedral sites of type A lead to a maximum value of 3.11 Å.

These constraints (equations A7 to A11) for the interstitial radius of type (b) sites are plotted in figure A5, resulting in $y = r_B = 2.65$ Å.

The radius of the octahedral sites are constrained only by the six neighbouring C_{60} molecules. The equations of constraint for the interstitial sites of type (c) are,

$$r_C \leq a/2 - r_{C60} \tag{A12}$$

and,

$$r_C \leq \sqrt{(a/2)^2 + (c/2)^2} - r_{C60} \tag{A13}$$

resulting in $r_C = 2.85$ Å..

For type (d) interstitial sites,

$$r_D \leq c/2 - r_{C60} \tag{A14}$$

$$r_D \leq \sqrt{(a/2)^2 + (a/2)^2} - r_{C60} \tag{A15}$$

leading to $r_D = 2.66$ Å for the largest possible interstitial radius.

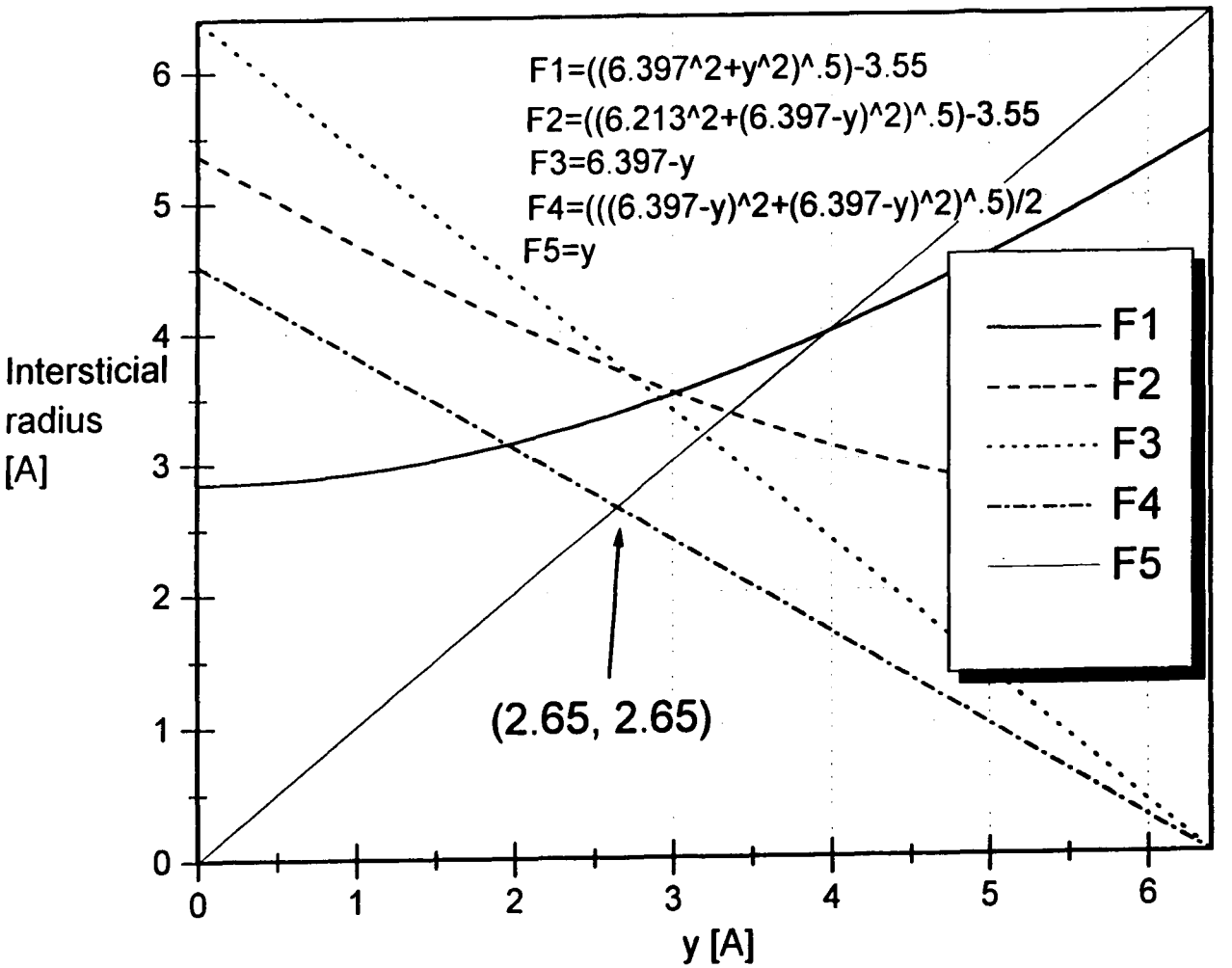

Fig. A5 Constraints on the radius of tetrahedral sites of type B lead to a maximum value of 2.65 Å.

REFERENCES

G. Begun and A. Rutenberg, *Inorg. Chem.* **6**, 12, 2213 (1967).

D.S. Bethune, G. Meijer, W.C. Tang, H.J. Rosen, W.G. Golden, H. Seki, C.A. Brown, and M.S. de Vries, *Chem. Phys. Lett.* **179**, 181 (1991).

I.D. Brown, McMaster University, private communication (1996)

B. Chase, N. Herron, and E. Holler, *J. Phys. Chem.*, **96**, 4262, (1992).

F. Chung and S. Sternberg, *American Scientist*, **81**, 56, (1993).

R.J.H. Clark, and D.M. Rippon, *Chem. Commun.*, 1295 (1971).

R.J.H. Clark, and D.M. Rippon, *J. Mol. Spectrosc.*, **52**, 58 (1974).

J. R. D. Copley, D. A. Neumann, R. L. Capelletti, and W. A. Kamitakahara, *J. Phys. Chem. Solids* **53**, 1353 (1992).

W.R. Datars, T.R. Chien, R.K. Nkum, and P.K. Ummat, *Phys. Rev. B.*, **50**, 4937 (1994).

W.R. Datars and P.K. Ummat, *Solid State Commun.*, **94**, 649 (1995).

C.G. Davies, P.A.W. Dean, R.J. Gillespie, P.K. Ummat, *Chem. commun.* **782** (1971).

G. Dresselhaus, M. S. Dresselhaus, and P. C. Eklund, *Phys. Rev. B* **45**, 6923 (1992).

A.F. Hebard, M.J. Rosseinsky, R.C. Haddon, D.W. Murphy, S.H.Glarum, T.T.M. Plastra, A.P. Ramirez, and A.R. Kortan, *Nature* **350**, 600 (1991).

J. Fischer, P. Heiney, A. McGhie, W. Romanow, A. Denenstein, J. McCauley, A. Smith, *Science*, **252**, 1288 (1991).

K. Hedberg, L. Hedberg, D. S. Bethune, C. A. Brown, H.C. Dorn, R.D. Johnson, and M. deVries, *Science*, **254**, 410 (1991).

G. Herzberg, *Molecular Spectra and Molecular Structure*, Vol. I: *Spectra of Diatomic Molecules*, Van Nostrand, Princeton, N.J., 1950

R. D. Johnson, C. S. Yannoni, H. C. Dorn, J. R. Salem, and D. S. Bethune, *Science* **255**, 1235 (1992).

W. Krätschmer, L. Lamb, K Fostiropoulos, D. Huffman, Nature, **347**, 354 (1990).

H.W. Kroto, J.R. Heath, S.C. O'brien, R.F. Curl, and R.E. Smalley, *Nature*, **318**, 162 (1985).

H Kuzmany, R Winkler, and T Pichler, *J. Phys.: Condens. Matter*, **7**, 6601 (1995).

M.C. Martin, D. Koller, L. Mihaly, *Phys. Rev. B*, **47**, 14607, (1993).

D. Maillard, M. Allevena, and J.P. Perchard, *Spectrochim. Acta.*, **31A**, 1523 (1975).

G. Mitra, *J. Am. Chem.Soc.*, **80**, 5639 (1958).

L.R. Narasimham, D.N. Stoneback, A.F. Hebard, R.C. Haddon, C.K. Patel, *Phys. Rev. B.*, **46**, 2591 (1992).

C. Naulin and R. Bougon, *J. Chem. Phys.*, **64**, 4155 (1976).

J.U. Nebgen, A.D. McElroy and H.F. Klodowski, *Inorg. Chem.*, **4**, 1796 (1965).

T. Pichler, M. Matus, and H. Kuzmany, *Solid State Commun.*, **86**, 221 (1993).

T. Pichler, R. Winkler and H. Kuzmany, *Phys. Rev. B*, **49**, 15879 (1994).

A.A. Quong, M.R. Pederson, and J.L. Feldman, *Solid State Commun.* **87**, 535 (1993).

C. Reber et al., *J. Phys. Chem.* **95**, 2127 (1991).

M. J. Rice and H. Y. Choi, *Phys. Rev. B.*, **45**, 10173 (1992).

E. Subbarao, D. Chakravorty, M. Merriana, V. Raghaven, L. Singhal, Experiments in Materials Science, McGraw-Hill, New York, 1972.

K. Tanigaki, T. Ebbeson, S. Saito, J. Mizuki, J. Tsai, Y. Kubo, and S. Kuroshima, *Nature* **352**, 222 (1991).

K. A. Wang, A.M. Rao, P.C. Eklund, M.S. Dresselhaus, and G Dresselhaus, *Phys. Rev. B*, **48**, 11375.

L.Wang, J. Conceicao, C. Jin, and R. Smalley, *Chem. Phys. Lett.*, **182**, 5 (1991).

Y. Wang, D. Tománek, G Bertsch and R. Ruoff, *Phys. Rev. B*, **47**, 6711 (1993).

R. Winkler, T. Pichler, H. Kuzmany, *Z. Phys.*, **96**, 39 (1994).

R. Winkler, T. Pichler, H. Kuzmany, *Appl. Phys. Lett.*, **66**, 1211 (1995).

D. Weeks and W. Harter, *J. Chem. Phys.* **,90**, 4744 (1989).

C. S. Yannoni, R. D. Johnson, G. Meijer, D. S. Bethune, and J. R. Salem, *J. Phys. Chem.*, **95**, 518 (1991).

R. Yoo, B. Ruscic, and J. Berkowitz, *J. Chem. Phys.*, **96**, 911 (1992).